Journal Pre-proof

IQ-RKT Bioactive formulation mitigates cardiomyocytes injury by targeting AGEs-RAGE-ROS-dependent TRAF3IP2/JNK apoptotic nexus

Humera Jahan, Urooba Fatima, Sana Asad, Sidra Zahoor, Priya Tufail, Dania Zainab, Nimra Naz Siddiqui, Aaqib Ullah, Marina Pizzi, M.Iqbal Choudhary

PII: S0891-5849(26)00004-3

DOI: https://doi.org/10.1016/j.freeradbiomed.2026.01.004

Reference: FRB 17550

To appear in: *Free Radical Biology and Medicine*

Received Date: 12 November 2025

Revised Date: 31 December 2025

Accepted Date: 3 January 2026

Please cite this article as: H. Jahan, U. Fatima, S. Asad, S. Zahoor, P. Tufail, D. Zainab, N.N. Siddiqui, A. Ullah, M. Pizzi, M.I. Choudhary, IQ-RKT Bioactive formulation mitigates cardiomyocytes injury by targeting AGEs-RAGE-ROS-dependent TRAF3IP2/JNK apoptotic nexus, *Free Radical Biology and Medicine*, https://doi.org/10.1016/j.freeradbiomed.2026.01.004.

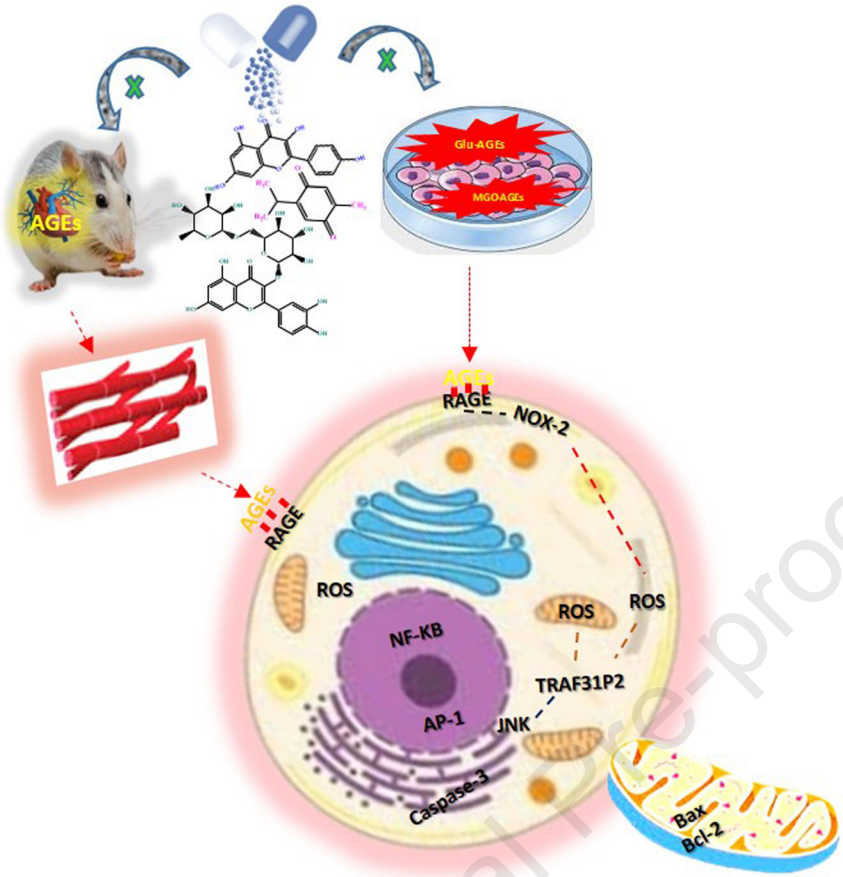

Title: **IQ-RKT Bioactive formulation mitigates cardiomyocytes injury by targeting AGEs-RAGE-ROS-dependent TRAF3IP2/JNK apoptotic nexus**

Humera Jahan[1,6]*, Urooba Fatima[1†], Sana Asad[1†], Sidra Zahoor[1], Priya Tufail[1], Dania Zainab[1], Nimra Naz Siddiqui[1], Aaqib Ullah[2], Marina Pizzi[5], and M. Iqbal Choudhary[1,2,3,4,6]*

[1]Dr. Panjwani Center for Molecular Medicine and Drug Research, International Center for Chemical and Biological Sciences, University of Karachi, Karachi-75270, Pakistan

[2]H.E.J. Research Institute of Chemistry, International Center for Chemical and Biological Sciences, University of Karachi, Karachi-75270, Pakistan

[3]Department of Chemistry, Faculty of Science and Technology, Universitas Airlangga, Komplek Kampus C, Jl. Mulyorejo, Surabaya-60115, Indonesia

[4]Institute of Drug Discovery Technology, Ningbo University, Ningbo-315211, China

[5]Department of Molecular and Translational Medicine, University of Brescia, Brescia 25123, Italy

[6]Institute of Molecular Biology and Biotechnology, The University of Lahore, Lahore-54000, Pakistan

†Both authors contributed equally.

Short Running Title: **Preventing cardiomyocytes apoptosis *via* repressing ROS-dependent TRAF3IP2/JNK signaling**

* Corresponding authors:

Tel.:+92-21-111-222-292; Fax: +92-21-99261713.

E-mail address: humerajahan@iccs.edu; jahan_pcmd@yahoo.com (H. Jahan)

Tel.:+92-21-111-222-292; Fax: +92-21-99261713.

E-mail address: iqbal.choudhary@iccs.edu; iqbalhej@yahoo.com (M.I. Choudhary)

HIGHLIGHTS

- A multicomponent natural formulation, IQ-RKT, was developed as an anti-apoptotic agent.
- AGEs induce cardiomyocytes apoptosis *via* ROS-dependent TRAF3IP2/JNK signaling.
- IQ-RKT reverses the AGEs-induced cardiomyocytes death *in vitro,* and *in vivo*.
- IQ-RKT improves the glucose metabolism in non-diabetic rats.
- IQ-RKT is a stable formulation at different pH, and temperature range.
- ^{1}H-NMR spectra of IQ-RKT showed no intermolecular interactions among the constituents.

ABSTRACT

Cardiovascular diseases (CVDs) are the leading cause of morbidity and mortality in diabetic populations. Elevated advanced glycation end products (AGEs) in diabetes foster the on-set, and progression of CVDs. However, the underlying AGEs-induced signaling nexus, involved in cardiomyocytes apoptosis, remain unexplored, and currently no anti-AGE drug available to address CVDs in diabetes. Indeed, natural products remained a major sources of modern medicine, and currently being recognized in the drug development. The objective of this study was to explore the mechanism of AGE-associated apoptotic pathway in cardiomyocytes. Additionally, to harness the medicinal properties of natural products, a newly developed formulation, comprised of rutin, kaempferol, and thymoquinone, named IQ-RKT, was characterized for its anti-apoptotic potential. We studied the role of MGO-, and glucose-AGEs in cardiomyocytes apoptosis under diabetic environment in H9c2 cells *in vitro*, as well as in SD diabetic rats *in vivo*. The inhibition of AGEs-induced apoptosis of cardiomyocytes was investigated by a treatment with IQ-RKT. Using H9c2 cells, as well as SD diabetic rats models *in vivo*, we found that AGEs-induced elevated levels of RAGE was reduced by a treatment with IQ-RKT. AGEs stimulate intracellular ROS generation, TRAF3 interacting protein 2 (TRAF3IP2) expression, and TRAF3IP2-dependent-JNK activation. TRAF3IP2/JNK causes transactivation of AP-1/NF-κB transcription factors. AGEs increase Bax, cytochrome c, and caspase-3 activation, and suppress anti-apoptotic Bcl-2. IQ-RKT significantly inhibited this apoptotic pathway, and tilted the balance towards anti-apoptosis. Moreover, IQ-RKT decreased lipid peroxidation, cardiac injury, and glycooxidative biomarkers in the plasma of diabetic rats. Interestingly this effect of IQ-RKT was independent of hyperglycemic environment in diabetic rats. The IQ-RKT also appeared as a stable formulation at different pH, and temperature ranges. The study provides experimental evidence that AGE-RAGE axis is associated with cardiomyocytes death *via* ROS-dependent TRAF3IP2/JNK pathway. Therefore, targeting this pathway, the developed formulation IQ-RKT identified as an effective anti-apoptotic cardioprotective agent to be further investigated through clinical studies.

Keywords: Apoptosis; Advanced glycation end products; Cardiovascular diseases; Oxidative stress; TRAF3 interacting protein 2; Natural product formulation IQ-RKT

INTRODUCTION

Cardiovascular diseases (CVDs), where the blood vessels and heart are negatively impacted, are the major cause of mortality in patients with diabetes, causing two-third of deaths [1,2]. There is a 2-4-fold higher risk of CVDs in diabetic patients, as compared to non-diabetic individuals[3,4]. In addition, the risk of developing cardiovascular complications is alike in both types 1, and 2 diabetes, irrespective of age and gender [5,6].

Elevated blood sugar levels in diabetes result in accelerated non-enzymatic glycation, oxidative stress, and carbonyl stress (elevated highly reactive diacarbonyl protein adducts, such as 3-deoxyglucosone (3-DG), glyoxal (GO), and methylglyoxal (MGO)). These processes lead to the formation of advanced glycation end products (AGEs), and advanced oxidation protein products (AOPPs). AGEs are the products of non-enzymatic glycation of biological macromolecules, such as proteins, lipids, and nucleic acids[7]. Like AGEs, elevated AOPPs (oxidatively modified dityrosine cross-linking protein products) also contribute in the pathogenesis of CVDs[8]. AGEs have a major role in the development of macro- and micro-vascular late complications in diabetes, such as myocardial infarction, stroke, retinopathy, nephropathy, and neuropathy[9,10]. AGEs play a critical role in metabolic memory because of their slow turnover rate which leads to their accumulation in the tissues, even after blood glucose levels are normalized[11]. Moreover, auto-oxidation of monosaccharides or carbonyl compounds through reactive oxygen species (ROS) or transition metals are also involved in AGEs formation[7].

AGEs have a major pathophysiological role in the on-set, and progression of CVDs in diabetic patients through the alteration of structures, functions, and mechanical properties of intra- and extra-cellular matrix proteins of tissues. AGEs also modulate cellular processes by binding to cell surface RAGE (receptors for AGEs)[12]. Elevated serum levels of AGEs are associated with the heart failure, both indirectly through their vascular effects (coronary dysfunction, atherosclerosis, and thrombosis), and through the direct actions on cardiomyocytes. AGEs signal *via* RAGE that are expressed on cardiovascular cells. AGEs-RAGE ligation leads to enhanced production of inflammatory cytokines, surface adhesion molecules, and activation of pro-apoptotic pathway[10,12,13].

The AGEs are the products of chronic hyperglycemia, and oxidative stress. They elicit intracellular oxidative stress by activating NOX (NADPH oxidase) family of NADPH oxidases in a variety of cell types[9,10]. NOX -2, and -4, isoforms of NOX oxidase, principally express in cardiomyocytes, and catalyze the generation of superoxide ($O_2^{\bullet}$), and hydrogen peroxides (H_2O_2). The ROS generation *via* NOX oxidases perpetuates their own production by a feed-forward mechanism, thereby contributing to chronic oxidative stress, and cells injury[10].

The redox sensitive transcription factors NF-κB (nuclear factor kappa-light-chain-enhancer of activated B cells) and AP-1 (activator protein-1), which regulate the life-death switch of a cell, have attracted major research interest in molecular biology. NF-κB normally acts as cytoprotective in heart, as it activates cell survival pathway under physiological conditions, but can be pro-apoptotic, depending upon the stimulus. Its role has been studied in cardiac pathologies[14]. Alternatively, AP-1, comprised primarily of c-Fos/c-Jun heterodimers, leads to cell injury, and death under oxidative stress environment[10].

A redox sensitive novel adaptor molecule TRAF3 (Tumor necrosis factor receptor-associated factor 3) interacting protein 2 (TRAF3IP2) physically attaches with IL-17RA, and contributes to IL-17A-mediated cardiomyocytes death[15,16]. IL-17A role has been studied in ischemic heart diseases (IHD), associated with cardiomyocytes death[17]. Ubiquitination of TRAF6 (Tumor necrosis factor receptor associated factor 6) at Lys63 by TRAF3IP2 activates IKK/NF-κB- and JNK (c-Jun N-terminal kinase)/AP-1-dependent cell death signaling[10,16]. Studies have identified TRAF3IP2 gene in alleviating hyperglycemia-induced cardiomyocyte apoptosis. However, the specific mechanism of how AGEs influence cardiomyocyte survival through the TRAF3IP2 remains unexplored [18,19]. Because of the increased systemic levels of AGEs in various chronic inflammatory diseases, including atherosclerosis, chronic kidney diseases, and diabetes, we hypothesized that AGEs affect the cardiomyocytes survival *via* ROS dependent TRAF3IP2/JNK activated NF-κB/AP-1 signaling pathway. Therefore, a detailed mechanistic study was performed on H9c2 (rat cardiomyocytes) cells under *in vitro* diabetic environment using MGO-AGEs, and glucose-AGEs models, as well as in *in vivo* Sprague-Dawley (SD) diabetic rat model. MGO is a dicarbonyl highly reactive intermediate that forms AGEs much faster (hours to days) *in vitro*. It represents a carbonyl stress state, which is observed in diabetes. In contrast, the *in vitro* glucose model mimics

a slow, long-term accumulation of AGEs under hyperglycemic milieu. The glucose-AGEs formation takes weeks to year in their formation *in vivo*[7,20].

Currently, there is no treatment available to address the detrimental effects of AGEs in diabetes, including the associated risk of CVDs. Phytochemicals have significant therapeutic potential[21]. They exhibit a wide range of pharmacological properties, including anti-cancer, anti-oxidant, anti-inflammatory, cardioprotective, and neuroprotective effects[22]. Exploiting the beneficial effects of bioactive constituents, we optimized a formulation, comprised of rutin, kaempferol, and thymoquinone; named IQ-RKT, to target the AGEs-associated apoptotic nexus in cardiomyocytes. Rutin is a bioactive flavonoid that exhibits anti-oxidant, anti-inflammatory, and cardiovascular properties. It has also been reported to inhibit lipopolysaccharide (LPS)-induced inflammation against the TRAF6-mediated signaling nexus[23]. Kaempferol is a flavonol, and reported to have cardioprotective properties in various heart tissue injury models. However, limited solubility and stability of flavonoids restrict their pharmaceutical uses[24]. Benzoquinones are known for their pharmacological applications, such as anti-cancer, anti-oxidant, etc[25]. For instance, thymoquinone is a benzoquinone, primarily sourced from black cumin seeds (*Nigella sativa*). It possesses anti-cancer and anti-inflammatory properties *via* suppressing NF-κB signaling pathway[26].

This study thus not only identified a mechanism of AGEs-associated cardiomyocytes apoptosis, but also report an anti-apoptotic agent, capable of preventing diabetic cardiotoxicity *via* inhibiting ROS dependent TRAF3IP2/JNK signaling pathway.

MATERIALS AND METHODS

Chemicals, reagents, and antibodies

Kaempferol (98%; A272671), thymoquinone (99%; A263475), aminoguanidine hydrochloride (98%; A287191), doxorubicin (A130952), and SP600125 (A155219) were purchased from Ambeed (USA). Metformin-HCL (PH1048), rutin (95%; R2303), bovine serum albumin (BSA; A3294), fetal bovine serum (FBS; F9665), D-(+)-glucose, eosin y-solution 0.5% aqueous (109844), and Papanicolaou's solution 1a Harris' hematoxylin solution (1.09253) were all obtained from Sigma-Aldrich (USA). Dulbecco's Modified Eagle Medium (DMEM; 52100-039), trypsin-EDTA (0.25%;

25200056), and Dulbecco's Phosphate Buffered Saline (DPBS) were purchased from Gibco (USA). 3-(4,5-Dimethyl-2-thiazolyl)-2,5-diphenyl-2*H*-tetrazolium bromide (MTT; A272671; 0.5mg/L for 4h) was purchased from SERVA Electrophoresis GmbH (Germany). ROTI® immunoblocking reagent (T144.1) was obtained from Carl Roth (Germany). Acetylated-NF-κB p65 (Lys310), Bax (MA5-14003), Bcl-2 (MA5-11757), RAGE (PA1-075), phospho-c-Jun (Ser63; MA5-15115), c-Jun (MA5-15172), TRAF3IP2 (PA5-22801), JNK1/JNK2/JNK3 (MA5-31974), phospho-JNK1/JNK2/JNK3 (Thr183, Tyr185; 44-682G), donkey anti-rabbit IgG (H+L)-Alexa Fluor 594 (A-21207), and- Alexa Fluor 488 (A-21206), antibodies, 2', 7'-dichlorofluorescein diacetate probe (DCFHDA; C6827), CellEvent™ Caspase-3/-7 green detection reagent (C10423), cytochrome c ELISA kit (KHO1051), and cell culture supplies were all purchased from Invitrogen (USA). Active caspase-3 (D260009) was from Sangon Biotech (China). Caspase-3 (PAA626Hu01), beta actin (ACTB; PAB340Mi01), and HRP-linked guinea pig anti-rabbit IgG (SAA544Rb59) antibodies, ELISA kits for advanced glycation end product (AGE; CEB353Ge), advanced oxidation protein products (AOPP; CEB223Ra), lactate dehydrogenase (LDH; SEB864Ra), glycated albumin (GA; CEA320Hu) cardiac troponin I (cTnI; SEA478Ra), and creatine kinase MB isoenzyme (CKMB; SEA479Ra) were procured from Cloud-Clone Corp (China). Antioxidant enzyme (glutathione (GSH; ELK8577), superoxide dismutase (SOD; ELK8178), and catalase (CAT; ELK5986) kits were obtained from ELK Biotechnology (China). AGE antibody (ab23722), and PDTC (ab141406) were from abcam (UK). Rat Hemoglobin A1c (HbA1c) colorimetric assay kit (80300) was purchased from Crystal Chem (USA). Transcription factor assay kits (TransAM® AP-1 family kit (44296), and TransAM® NF-kB family kit (43296) were obtained from Active Motif (USA). The RIPA (radio-immunoprecipitation assay) lysis buffer system (sc-24948A), and apocynin (sc-203321) were purchased from Santa Cruz Biotechnology (USA), and camptothecin (22069) was obtained from Chem-Impex International (USA). Rotenone (150154) was purchased from MP Biomedical (France). The chromogenic LAL assay kit was purchased from Invitrogen (USA). H9c2 cell line was obtained from American Type Culture Collection (ATCC, USA). Streptozotocin (STR-201) was purchased from BioShop (Canada). Locally available edible olive oil (100%; *Sassu*, Italy) was purchased to dissolve the test compounds.

***In vitro,* and *in vivo* study design and methods**

Culture of H9c2 embryonic cardiomyocytes, and *in vitro* experimental procedure

Rat embryonic cardiomyocytes cell line (H9c2) was cultured in a basal medium, Dulbecco's Modified Eagle's Medium (DMEM), supplemented with 10% (*v*/*v*) fetal bovine serum (FBS), L-glutamine, and sodium pyruvate (Figure 1). The culture was maintained in an aseptic humid optimal growing environment, *i.e*. 37° C; 5% CO_2, with frequent change of media every 2-3 days. Cultured H9c2 cells from passages 3 to 5 were used in all the experiments, as H9c2 rat cardiomyocytes are a reliable *in vitro* model till five passages[27]. Based on the designed experiments, cells were seeded at different densities in a low (5%) serum medium.

To mimic the diabetic environment, MGO- and glucose-AGEs were prepared, as reported previously by our research group[13]. Briefly, MGO-AGEs were prepared by incubating BSA (10 mg/mL) with MGO (100 mM) in a dark sterile environment for 24 h. While a mixture of glucose (500 mM), fructose (50 mM), and MGO (3 mM) were incubated with BSA (10 mg/mL) for 5 weeks to prepare glucose-AGEs. The pH was adjusted to 7.4 every week by adding NaOH (1 M). After incubation, both AGEs were dialyzed against 1X PBS. AGEs-specific fluorescence for MGO-BSA, and glucose-BSA was measured at an excitation and emission wavelengths of 355/460 nm, and 340/440 nm, respectively. Protein concentration was estimated *via* BCA assay kit, while endotoxins levels in the AGEs preparation was measured by LAL assay kit. The endotoxin levels were found to be < 0.01 EU/mL. Both AGEs were stored at -80° C until use. For the treatment procedure, initially MGO- and glucose-AGEs, and test formulation IQ-RKT (an equimolar composition of Rutin, Kaempferol, and Thymoquinone) were tested at a broader concentration range 10-1000 µg/mL; and 10-1000 µM, respectively, by MTT metabolic assay to select the non-toxic concentrations for the experiments. Likewise, DCFH-DA probe was used to identify the stimulants (MGO- and glucose-AGEs), and test formulation (IQ-RKT) in optimal concentrations those inhibit the intracellular ROS ($O_2^{\bullet}$) generation.

The cell growth inhibitors doxorubicin (topoisomerase II blocker, 100 µM), and camptothecin (CPT, topoisomerase I inhibitor, 4 µM) were used as reference controls in viability, and apoptosis assays, respectively. BSA was used as a control for MGO- and glucose-AGEs.

For the signal transduction pathway studies, cells were pre-treated with IQ-RKT (10 µM), and different known inhibitors: apocynin (NADPH oxidase inhibitor, 100 µM), rotenone (mitochondrial electron transport inhibitor, 10 µM), PDTC (100 µM), and SP600125 (JNK inhibitor,

20 µM) (pathway controls), followed by stimulation with MGO-AGEs (300 µg/mL), and glucose-AGEs (Glu-BSA; 100 µg/mL) at different time intervals, based on the specific signaling molecule study. At the indicated concentrations of pharmacological inhibitors, no detectable phenotypic modulation of H9c2 cardiomyocytes, and adherence to culture plates were observed. Each experiment was run in triplicate.

H9c2 Cardiomyocytes viability and death assays

To examine whether formulation IQ-RKT modulate the cardiomyocytes viability, under AGEs treatment, we analyzed the cell viability using the MTT metabolic assay, as described previously[28]. H9c2 cells at a density of 18 x 10^4 cells/mL were seeded overnight in a 96-well cell culture plate. Following adherence to the plate, cells were pre-treated with formulation IQ-RKT at various selected concentrations (10, 30, and 50 µM) for an hour, then incubated with MGO-, and Glu-AGEs for 24 h.

Following formula was used to measure cell viability percentage:

Cell viability (%) = $[(A_T - A_b) / (A_c - A_b)] \times 100$ (where: A absorbance; $_T$ test; $_c$ control; $_b$ blank).

The cardiomyocytes death was investigated through morphological aspects using H&E staining. Cells (30 x 10^4 cells/mL) were pre-treated with IQ-RKT (10 µM), co-incubated with MGO-, and Glu-AGEs for 24 h in a 24-well plate. In brief, cells were fixed with paraformaldehyde (4%) for 10 min, stained with eosin for 1 min, and then with hematoxylin for 30 sec, and washing thrice in each step with 1X PBS.

In addition, the cell death was detected *via* quantifying cytochrome c levels using cytochrome c ELISA kit. This assay is based on solid-phase sandwich ELISA principle, using a capture antibody directed against cytochrome c. This allows the specific detection of cytochrome c that is released into the cytoplasm of cells undergoing apoptosis upon incubation with MGO-, and Glu-AGEs. All the components were provided in the kit. After an hour treatment with IQ-RKT (10 µM), cells (1 x 10^6 cells/mL) were incubated with MGO-, and Glu-AGEs for 6 h before analysis. Briefly, lysate from treated and untreated controls, and standards were transferred to the precoated ELISA plate, and incubated with a biotinylated detection antibody. The plate was washed, as recommended in the protocol, and incubated with streptavidin-HRP to generate signals.

Following washing, chromogenic substrate was added, and absorbance was measured at 450 nm (Varioskan LUX multimode microplate reader, Thermo Fisher Scientific, USA).

Cardiomyocytes ROS detection

Intracellular ROS generation was evaluated by DCFH-DA (general oxidative stress indicator) technique, as previously described[29]. Cells were pre-treated with IQ-RKT at 10, 30, and 50 µM concentration, and incubated with MGO-, and Glu-AGEs for 24 h. Following subtraction of background fluorescence, data was represented as RFU/18 x 10^4 cells.

TransAM DNA-binding ELISA

The major transcription factors AP-1 and NFκB translocation and DNA-binding activities were detected through TransAM AP-1 family, and TransAM NF-kB family kits. In brief, nuclear extracts were prepared, following the treatment of H9c2 cells (1.5 x 10^6 cells) with IQ-RKT (10 µM), and MGO-, and Glu-AGEs for 1 h. TransAM assays were performed in accordance with the manufacturer protocol using 8 µg/well extracts from controls and treated wells with the c-Fos, FosB, JunD, and phospho-c-Jun antibodies for AP-I assay, while p65, and c-Rel antibodies for NF-kB assay. The results were calculated as the change in the OD at 450 nm over µg of total protein extracts.

Caspase-3/-7 activation assay

A fluorogenic substrate was used to detect the activated caspase-3 and -7 in the cardiomyocytes by employing end point apoptotic assay using CellEvent™ Caspase-3/-7 Green Detection Reagent. In brief, H9c2 cells (18 x 10^4 cells) after treatment with IQ-RKT (10 µM) and MGO-, and Glu-AGEs for 4 h in a 96-well cell culture plate were incubated with a fluorogenic substrate (7.5 µM) for 30 min at 37° C. The live cells fluorescence was recorded at the excitation emission maxima 502 nm/530 nm (Varioskan LUX multimode microplate reader, Thermo Fisher Scientific, USA). Next, cells were fixed with formaldehyde (3.7%), and counterstained with DAPI for 2 min for fluorescence imaging *via* Nikon Ti-2 fluorescence microscope equipped with DXM-1200 digital camera. Images were analyzed with NIH ImageJ software.

***In vivo* study design, and experimental procedure**

Experimental animals and ethical approval: Albino male rats, SD, 8-10 weeks old, weight = 220 ± 20 g, were purchased from the National Facility for Laboratory Animal Research and Care (NFLARC, ICCBS), and housed in a relative humidity of 40 - 50% at 24-25° C ± 1° C under a 12h light/dark environment. Animals were fed with standard chow diet, and water *ad libitum* during the entire course (12 weeks) of the study. All procedures were followed according to the Guide for the Care and Use of Laboratory Animals, 8th edition, National Research Council (US), and were approved by the Institutional Animal Care and Use Committee (*IACUC,* Study Protocol No. ICCBS-ASP-10-2022-013).

Diabetes induction in experimental rats: Animals were acclimatized to the laboratory conditions, prior to the induction of diabetes. Diabetes was induced as described previously[30], with slight modifications in the protocol. In brief, rats were subjected to 12 h of fasting, and then diabetes induced by single intraperitoneal injection of streptozotocin (STZ, 45 mg/kg) (type 1 diabetic model), while control (normal rats) was injected only with vehicle, citrate buffer (Figure 1). Rats were kept overnight on glucose solution 5% (*w*/*v*) to avoid hypoglycemia. Fasting blood glucose (FBG) levels were monitored after 72 h, and one week *via* tail prick glucometer method. Rats with FBG > 200 mg/dL, along with the clinical signs of diabetes, were selected for the study.

Rational of maximum tolerated dose selection: The therapeutic dose of IQ-RKT formulation was initially determined in STZ-induced diabetic rats. IQ-RKT (a 1/3 composition of Rutin, Kaempferol, and Thymoquinone dissolved in olive oil) was daily administered orally for 5 weeks at different doses, such as 10, 50, and 100 mg/kg/b.w. (n = 6/group), based on toxicity studies. A dose dependent significant cardioprotective effect (data not shown) was observed at 50 mg/kg dose with improved body weight, left ventricular ejection fraction (LVEF), and decreased AGEs and malondialdehyde (MDA) levels, independent of blood sugar levels. While, 100 mg/kg dose showed similar effects, therefore, 12 weeks study was conducted with a lower formulated composition 50 mg/kg to attain maximum beneficial effect without any adverse effects.

Experimental protocol: Rats were randomly divided into seven groups (n = 12/group). Group 1: nondiabetic controls (ND); group 2: diabetic controls (D); group 3: diabetic rats treated with standard aminoguanidine (50 mg/kg/d)[31,32] (D+AG); group 4: diabetic rats treated with rutin (16.6 mg/kg/d) (D+R); group 5: diabetic rats treated with kaempferol (16.6 mg/kg/d) (D+K); group 6:

diabetic rats treated with thymoquinone (16.6 mg/kg/d) (D+T); and group 7: diabetic rats treated with IQ-RKT (50 mg/kg/d) (D+ IQ-RKT). Treatment (groups 3-7) was started after one week of diabetes confirmation, and continued for consecutive 12 weeks. If needed, insulin (Humulin 70/30, 2 U/day) was subcutaneously injected to the diabetic rats with elevated glycemic levels (> 500 mg/dL) to prevent acute complications, such as diabetic ketoacidosis (DKA).

At the end of the treatment, rats were anesthetized with intraperitoneal ketamine (100 mg/kg), and xylazine (2 mg/kg). Blood samples were collected *via* cardiac puncture in EDTA tubes, and analyzed for biochemical, and molecular markers. Moreover, internal organs were isolated for histopathological examination, and for oxidative stress and molecular studies.

Body weight and glycemic parameters

During the entire study period, body weight and FBG levels were monitored on weekly basis. HbA1c levels were quantified at the end of the study using rat hemoglobin A1c (HbA1c) assay kit in accordance with the manufacturer protocol. In addition, glycated albumin levels were determined using ELISA kit. In brief, sandwich-ELISA method was applied using capture antibody, specific to glycated albumin, and HRP-conjugated detection antibody. The absorbance was measured at 450 nm (Varioskan LUX multimode microplate reader, Thermo Fisher Scientific, USA), following addition of chromogenic substrate.

Glycooxidative stress biomarkers assessment

The levels of glycooxidative stress markers, AGEs (a biomarker of glycemic and oxidative stress[33]), and AOPPs (a biomarker of oxidation-associated protein damage[34]), were quantified in the plasma *via* ELISA (competitive ELISA) kits. In brief, competitive inhibition reaction was initiated between biotin labelled- AGEs, and AOPPs, and unlabeled samples with the AGEs-, and AOPPs-specific antibodies (pre-coated). After washing, avidin-HRP was added. Next, chromogenic substrate was added, and the intensity of color was measured at 450 nm (Varioskan LUX multimode microplate reader, Thermo Fisher Scientific, USA). In addition, protein carbonyl (protein-carbonyl adducts under oxidative stress[35]) contents, and malondialdehyde (MDA) (a lipid peroxidation marker[36]) levels were determined in the heart homogenate (10 mg/500 µL). The 2,4-dinitrophenylhydrazine (DNPH) colorimetric assay was employed to quantify carbonyl

contents at 370 nm, and results were expressed as nmol/mL. The malondialdehyde (MDA) or thiobarbituric acid reactive substances (TBARS) were determined by a colorimetric assay, and absorbance was recorded at 532 nm (Varioskan LUX multimode microplate reader) (Thermo Fisher Scientific, USA). The data was presented in µM.

Antioxidant enzymes assessment

The levels of antioxidant enzymes, glutathione (GSH), superoxide dismutase (SOD), and catalase (CAT), were determined in heart lysate. The protein concentration was estimated with BCA protein assay kit. GSH Levels were quantified using ELISA kits based on competitive inhibition- and SOD and CAT on sandwich- enzyme immunoassay principles. The user manuals were strictly followed. The data for GSH was expressed in pg/mL, while SOD, and CAT measured in ng/mL.

Cardiac markers detection

The cardiac markers that signifies cardiomyocytes death[37], such as LDH, CK-MB, and cTnI, were detected in the plasma by LDH, CK-MB, and cTnI ELISA, based on sandwich immunoassay principle. The LDH, and CK-MB results were expressed in ng/mL, while cTnI in pg/mL.

Histopathological examination

For histopathological study, harvested organs, including heart, kidney, and pancreas, were incised into multiple sections, fixed in formalin (3.7%), embedded in paraffin, and stained with hematoxylin-eosin (H&E) using previously described method[5]. The sections, 5 µm (thickness), from each specimen were observed for gross structural and cellular details by the pathologist. Further, paraffin-embedded specimens from heart and kidney were also stained with Masson's trichrome to determine fibrosis using a standard method[38]. All the specimen slides were observed *via* NiE microscope (Nikon, Japan), equipped with DXM-1200 digital camera.

Immunoblotting

To evaluate the protein expression of targeted pathway, immunoblotting techniques were used. Extraction and preparation of tissue (10 mg)- and whole cell- lysates (1.5 x 10^6 cells) in RIPA lysis buffer, protein estimation *via* standard BCA assay, electrophoresis (50 µg protein from each sample resolved on 10% SDS-PAGE gel), and immunoblotting were all carried out, as described

previously[30]. β-Actin served as internal reference. ECL detection kit was used to visualize the bands, and densitometric analysis was carried out by using ImageJ software. Three biological replicates were performed of each targeted molecules.

Immunofluorescence imaging

Further, key molecular markers of the targeted pathway were analyzed at the cellular, and tissue levels *via* immunofluorescence imaging technique. In brief, H9c2 cells (30 x 10^4 cells/mL) were fixed by using paraformaldehyde (4%, 10 min), washed thrice (1X PBS, 5 min each), and permeabilized (0.2% Tritron X-100, 10 min). Whereas, heart specimens were fixed with neutral buffered formalin (3.7%), and dehydrated with graded series of alcohol for paraffin-embedding. Following deparaffinization and hydration steps, tissue antigens were retrieved with 10 mM citrate buffer (pH 6.0, 30 min) at 90° C. Cells, and heart specimens were blocked with 1% BSA (1 h), and 1X roti immunoblock (30 min). Next, treated with primary (AGEs, RAGE, TRAF3IP2, Bax, and Bcl-2)-, and probe labelled secondary- antibodies, counterstained, and mounted as described previously[30,39]. The images of cellular- and tissue specimen were captured by Nikon Ti-2, and NiE fluorescence microscopes, respectively, and analyzed by using ImageJ software. Six fields were selected from each group to plot a graph.

Hypoglycemic activity test

To investigate whether IQ-RKT formulation has any hypoglycemic effect, oral glucose tolerance test (OGTT)[40] was performed on normal healthy male SD rats (8-10 weeks old) (Figure 1). The standards (metformin, and aminoguanidine), formulation IQ-RKT (a 1/3 composition of each) were tested at three different concentrations, 10, 50, and 100 mg/kg. After adaptation period, rats were fasted overnight (12 h), and divided into 4 groups (groups I-IV). Groups II-IV were further divided into three sub-groups (n=5/group). Control group (group I) received only glucose (2 g/kg/b.w. orally), while standards (groups II-III), and test (IV) groups received treatment orally before 30 minutes of glucose administration. Finally, the blood glucose levels were measured at different intervals: 0 min (before glucose load), and then after glucose administration at 30, 60, 90, and 120 min by tail-prick method, using a glucose meter (Accu-Chek®, Roche).

Physicochemical stability study

Physicochemical stability study was performed to assess the pH, temperature, and structural variations which may disrupt their stability. The stability of novel composition IQ-RKT (a mixture of Rutin, Kaempferol, and Thymoquinone) was evaluated at various pH ranges *i.e.,* 2, 6, 7, 8, and 10 by ultraviolet-visible (UV-vis) spectrophotometer. The pH of the mixture was adjusted by adding diluted solution of HCl, and NaOH. Similarly, the formulation was also subjected to temperature effect at 25, 37, 40, and 50° C for 30 minutes, and their absorbance were recorded through UV-vis spectrophotometer. The effect of temperature by taking the mixture ^{1}H-NMR at 50° C was recorded in DMSO-d_6 at 400 MHz, on Bruker Avance NEO 400 Nuclear Magnetic Resonance Spectrometers, and compared with individual component.

Statistical analysis

Data was statistically analyzed *via* SPSS (V.27), and were represented as mean±SD. For comparison between controls and various treatments groups, one-way ANOVA was performed followed by post hoc Tukey's multiple comparisons test. Data was considered statistically significant at $p < 0.05$. GraphPAD Prism (V.8.0.2) was used for graphics.

RESULTS

IQ-RKT Reverses AGEs-induced cardiomyocytes death

We employed a quantitative and qualitative approaches to evaluate the cardioprotective effect of IQ-RKT *in vitro* under pathological concentrations of AGEs. Both AGEs, derived from methylglyoxal (MGO)-, and glucose (Glu)-modified BSA (10-1000 µg/mL), significantly lowered the viability of H9c2 cells, with a concentration as low as 10 µg/mL. A maximal inhibition of cells viability was observed at 300 µg/mL MGO-AGEs, while 100 µg/mL of Glu-AGEs (Figure S1). Further, both AGEs at 300 µg/mL, and 100 µg/mL, respectively, were also found to induce a higher ROS production in H9c2 cells (Figure S2). Whereas in similar conditions, unmodified BSA showed no effect on H9c2 cells viability. Hence, in subsequent experiments, AGEs were used at 300 µg/mL (MGO-AGEs) and 100 µg/mL (Glu-AGEs) concentrations as pathological stimulants. Likewise, to select non-cytotoxic concentration of IQ-RKT for further experiments, cytotoxicity at

10-1000 µM was assessed on H9c2 cells. At 10-50 µM, IQ-RKT treatment showed no significant effect on the viability, as compared to untreated cells (Figure S3). Whereas, cells viability significantly reduced (≤ 16%) at higher concentrations (100-1000 µM), comparable to standard, doxorubicin.

The effect of IQ-RKT on H9c2 cardiomyocytes viability was assessed by using MTT assay. This involved pre-treatment (60 min) of cells with IQ-RKT (10-50 µM), prior to exposing cells with AGEs stimulants for 24 h. The significant protective effect was observed at 10 µM (87% viability under MGO-AGEs; and 94% Glu-AGEs environment) (Figure 2A), as compared to AGEs controls. However, at 50 µM, IQ-RKT was not found effective against AGEs-induced cytotoxicity (69% MGO-AGEs; and 76% Glu-AGEs). Considering the optimal viability effect of IQ-RKT formulation under AGEs environment, IQ-RKT was studied *in vitro* at 10 µM.

The anti-cell death effect of IQ-RKT under AGEs treatment was investigated *via* H&E staining (Figure 2B). This showed morphological state of H9c2 cells after the treatment with BSA, MGO-, and Glu-AGEs, and IQ-RKT pretreatment. The cells lost their spindle morphology in both AGEs treatment (Figure 2Biii, 2Biv). Cells appeared in round shape after MGO-treatment (Figure 2Biii), while the nuclei condensation, along with pronounced size shrinkage, were observed in Glu-AGEs-treated specimen (Figure 2Biv). However, with IQ-RKT pre-treatment, cells retained their normal size and shape, and a highly organized cell connections were observed (Figure 2Bv, 2Bvi).

Further, IQ-RKT anti-apoptotic effect on cardiomyocytes were studied by quantifying cytochrome c (Cytc) levels (Figure 2C) *via* ELISA assay. The cell death, accompanied with the release of Cytc into the cytoplasm, triggers the apoptosome formation, and caspase activation[41,42]. MGO-, and Glu-AGEs treated H9c2 cells showed 2.3-, and 5.7-fold elevated signals of Cytc levels, as compared to untreated control cells. Whereas, IQ-RKT treatment significantly protected against the AGEs-mediated upsurge (1.8-fold MGO-AGEs; and 3.7-fold Glu-AGEs) in H9c2 cells. The treatment with JNK inhibitor SP600125 (anthra[1,9-cd]pyrazol-6(2H)-one) was found equally effective in decreasing (2.6-2.5-fold) the AGEs-mediated Cytc content. These results indicate that IQ-RKT has the potential to suppress the MGO-, and Glu-AGEs-mediated pro-apoptotic signals in cardiomyocytes.

IQ-RKT Lowered glycated albumin levels under diabetic environment

Aminoguanidine (AG), a prototype inhibitor of AGEs, mainly prevents the formation of AGEs by scavenging dicarbonyl compounds[43,44]. Despite its effect as an antiglycation agent, clinical trials were terminated due to safety concerns, and low efficacy of AG[43]. In our *in vivo* study after streptozotocin (STZ, 45 mg/kg) injection, a substantial decrease in body weight was observed initially in SD rats groups 2-7 (group 2: diabetic control (D); group 3: diabetic rats treated with standard aminoguanidine (D+AG); group 4: diabetic rats treated with rutin (D+R); group 5: diabetic rats treated with kaempferol (D+K); group 6: diabetic rats treated with thymoquinone (D+T); and group 7: diabetic rats treated with combination IQ-RKT (D+ IQ-RKT) (Figure 3A), an elevated blood glucose levels were observed during the entire study period of 12 weeks (Figure 3B), as compared to nondiabetic control (ND) group 1. While, no significant decrease in body weight was observed in treated groups (groups 4-7). Whereas, AG (group 3) treatment exhibited a significant decrease in body weight. Further, HbA1c levels were remained significantly higher (range 8-9%) in groups 2-7, as compared to the levels (4%) of control group 1 (Figure 3C).

In contrast, IQ-RKT significantly lowered the glycated albumin levels than diabetic control (Figure 3D), comparable to AG. It is previously reported that lowering of HbA1c and glycated albumin are independent to each other, and may follow different mechanisms[45]. Comparatively, rutin, kaempferol, and thymoquinone- treated diabetic groups had shown relatively weaker potential in lowering the glycated albumin levels, but their combination IQ-RKT significantly lowered the glycated albumin to a normal level, even showed a remarkable inhibition than AG.

IQ-RKT Inhibits glycooxidative stress markers under diabetic milieu

It is well documented that AGE-RAGE ligation induces ROS production in cardiomyocytes by involving NOX enzymes, and mitochondria[46,47]. Based on the reported antioxidant activities of three constituents, we hypothesized that IQ-RKT treatment can modulate the AGEs-induced intracellular oxidative stress. We observed that reference inhibitors of ROS, apocynin (NADPH oxidase inhibitor), and rotenone (mitochondrial electron transport inhibitor), ameliorated the AGEs-induced ROS generation in H9c2 cells, as detected by DCFH-DA probe. Similarly, IQ-RKT pre-treatment significantly attenuated both MGO-, and Glu-AGEs- stimulated ROS generation in H9c2 cells (Figure 4A).

Hyperglycemia in diabetes leads to oxidative stress, which is associated with the pathogenesis of macrovascular complications, including diabetic cardiomyopathy[48]. Malondialdehyde (MDA), a lipid peroxidation marker, and protein carbonyls adducts, are indicators of oxidative damage to proteins in cells. They also depict the disease states, such as cardiovascular diseases, diabetes, and neurodegenerative disorders[49,50]. We further investigated the effect of IQ-RKT on oxidative stress markers; protein carbonyl adducts, and MDA, in diabetic SD rats. AG (group 3), and treatment alone with rutin group (group 4), and kaempferol group (group 5) showed a significant decrease in the MDA levels in the heart tissues, than the diabetic control (group 2) (Figure 4B). While treatment with thymoquinone (group 6) exhibited some inhibitory effect, greater than the diabetic controls. Whereas, the IQ-RKT treatment (group 7) caused highly significant decrease in MDA levels among all the treatment groups. Although IQ-RKT treatment did not achieve the statistical significance in lowering the protein carbonyl stress in the heart tissues, the inhibitory effects appeared to be greater than diabetic control (Figure 4C). The treatment alone groups (groups 4, and 5) exhibited a weak inhibition, while group 6, and AG group 3 showed no inhibition. IQ-RKT showed a robust effect on protein carbonyl levels than treatment alone groups (groups 4-6).

Hyperglycemia, and dicarbonyl-and oxidative- stress accelerate the formation of AGEs in patients with diabetes. As AGEs are heterogeneous adducts, many are formed by the combination of oxidation and glycation, and hence are called as glycoxidation products[51]. Further, we determined the effect of IQ-RKT on AGEs and AOPPs levels in diabetic SD rats. IQ-RKT not only significantly reduced the AGEs plasma levels, as compared to diabetic control, but also exhibited a comparable reduction than the treatment alone-, and AG groups (Figure 4D). AG-treated rats had somewhat lowered the AGEs levels. Moreover, the accumulation of AGEs in the cardiac tissues was also investigated through immunohistochemistry and immunoblotting techniques. In diabetic SD rats, a marked increase (1.2-fold) of AGEs in the cardiac tissues was observed (Figure 4E (a, and b), and 4F (a, and b)), as compared to normal non-diabetic (ND) control. Whereas, IQ-RKT significantly lowered (1.3-fold) the tissue levels of AGEs among all the treatment groups, as compared to AG treatment group. AOPPs serve as an independent risk factor for ischemic heart diseases (IHD), associated with cardiomyocytes injury and death[10]. The significantly elevated plasma AOPPs levels in diabetic control were noticeably attenuated by IQ-

RKT treatment (Figure 4G). Except kaempferol (group 5) treatment alone, the rutin (group 4), and thymoquinone (group 6) treatments lowered the AOPPs levels. AG treatment also showed minor decreasing effect on plasma AOPPs levels. These results suggest that rutin, kaempferol, and thymoquinone functions more effectively in combination. As a result, IQ-RKT formulation was found effective in lowering the glycooxidative stress under diabetic environment, associated with diabetes cardiovascular complications.

AGEs increase oxidative stress by altering the structures and functions of antioxidant enzymes, which may also contribute to diabetic cardiomyopathy[52]. Therefore, we investigated the effect of IQ-RKT on the antioxidant enzymes in heart tissues of diabetic rats. Interestingly, IQ-RKT (group 7) significantly enhanced the levels of superoxide dismutase (SOD) enzyme, as compared to treatment with rutin alone (group 4), kaempferol (group 5), and thymoquinone (group 6) diabetic heart tissues (Figure 4H). Besides, SOD levels were found in normal range with IQ-RKT treatment like in ND control (group 1). Similarly, the levels of catalase (CAT) enzyme remained normal in IQ-RKT treated heart tissues, and treatment alone groups, as ND control (Figure 4I). While, the levels of SOD, and CAT enzymes were found lowered in AG (group 3) than the diabetic control (group 2). The glutathione (GSH) enzyme levels were also found normal in IQ-RKT heart tissues, while a slight decrease was observed in treatment alone groups 4-6 (Figure 4J). Whereas, AG significantly raised the levels of GSH enzyme, as compared to diabetic, and ND controls. These findings suggest that IQ-RKT treatment can protect the key antioxidant defense mechanism in the heart probably by virtue of its antioxidant, and cardioprotective properties.

IQ-RKT Suppresses cardiac markers associated with myocardial injury

We next investigated the effect of IQ-RKT, and each of its constituent on a range of cardiac markers, based on ELISA tests. The objective was to evaluate the myocardial injury under diabetic environment, and assess the protective effect of IQ-RKT, if any. Lactate dehydrogenase (LDH), an anaerobic glycolysis enzyme, serves as a marker of cardiac injury, and a risk factor for mortality in inflammatory diseases[53]. The significantly increased LDH levels in the plasma of diabetic rats (group 2) were remarkably suppressed by IQ-RKT treatment (group 7) (Figure 5A). Diabetic rats, treated with kaempferol (group 5), and thymoquinone (group 6), also significantly reduced the levels of LDH, while rutin treatment (group 4) did not show any suppressive effects. Besides, IQ-

RKT treatment also exhibited a significant LDH suppressive activity, as compared to the individual constituents' treatment groups (groups 4-6). AG (group 3) reduced the levels of LDH, but not as significant as by IQ-RKT.

We then determined a commonly used cardiac biomarker, creatine kinase-myocardial band (CK-MB), which was found significantly elevated in the plasma of diabetic rats (Figure 5B). Among the individual constituents' treatment groups (groups 4-6), only thymoquinone (group 6) was able to lower the elevated levels of CK-MB, while rutin (group 4), and kaempferol (group 5) treatments failed to reduce the elevated CK-MB levels. Whereas, IQ-RKT treatment resulted into a remarkable lowering of the CK-MB levels, as compared to the plasma levels of diabetic group. AG treatment also showed a significant inhibition effect.

Furthermore, a more specific cardiac biomarker, cardiac troponin I (cTnI), was also measured in the plasma of controls and treatment groups to assess the myocardial injury. The significant elevated levels of cTnI were noted in the diabetic group (group 2), while AG (group 3), individual component (groups 4-6), and IQ-RKT (group 7) treatments significantly lowered the cTnI levels (Figure 5C). IQ-RKT showed a more potent cTnI inhibitory effect than individual components treatments. Rather contradictory results on cardiac markers in groups 4, and 5, elevated CK-MB levels, but reduced cTnI levels, may be due to other disease states, such as renal insufficiency, and rhabdomyolysis, which was further ruled out through tissue examination. These findings suggested that IQ-RKT exhibits a cardioprotection.

IQ-RKT Prevents the cardiac muscles and kidney malfunction under diabetic milieu

The histopathological examination of various organs of experimental animals (SD rats), including heart, kidney, and pancreas, was performed to study the effect of IQ-RKT treatment at the gross tissue levels, as compared to the diabetic control. On H&E staining, the cardiac muscles cells (Figure 6A(a)) were seen to contain a branched eosinophilic cytoplasm with one or two nuclei (**N**) centrally located. The intercalated disc (**ID**) marked the intracellular boundaries, and intercellular spaces, filled with delicate supporting tissues, were also observed at 400x magnification in normal non-diabetic control (group 1). The branching pattern was found distorted in group 2 diabetic rats. Several focal regions with well demarcated round and cleared vacuoles (**V**) were noted, indicating degenerative process, and myocardial injury (Figure 6A(b)). AG-treated group 3

also prevented the cardiac tissues (Figure 6A(c)). As shown in Figure 6A(g), IQ-RKT treatment (group 7) showed a remarkable effect in preventing any diabetes-mediated insult on cardiomyocytes, with preserved capillary supply, as compared to the individual constituents' treatment groups (groups 4-6) (Figure 6A (d, e, and f)). The Masson's trichrome staining revealed that muscles fibers were bright red with increased fibrosis (**F**), and collagen (**C**) deposition in diabetic control (Figure 6B(b)), as compared to non-diabetic control (group 1) (Figure 6B(a)). As shown in Figure 6B(g)), IQ-RKT treatment prevented fibrosis under diabetes stressed environment, as compared to the individual treatment groups (groups 4-6) (Figure 6B (d, e, and f)). This reflects that these constituents in combination are more effective in preventing heart tissues under diabetes stress environment. A slight collagen deposition was observed in AG-treated group (Figure 6B(c)).

Upon histological examination (H&E, and Masson's trichrome staining) of kidney, normal renal corpuscle, a combination of Bowman's capsule (**BC**), and the glomerulus (**G**), proximal tubules (**PT**), and distal tubules (**DT**) size were observed in non-diabetic control (group 1) (Figure 6C(a)). Nuclei (**N**) of capillary endothelial cells, podocytes, and mesangial cells were seen in the glomerulus at 400x magnification. No collagen deposition was observed with Masson's trichrome staining 200x magnification (Figure 6D(a)). A marked expansion of Bowman's capsule, and dilated tubules (dT*) with interstitial fibrosis (**IF**) were seen in diabetic control (group 2) (Figure 6C(b)). Fibrosis, along with prominent loss of glomerular mass, is shown in Figure 6D(b). AG treatment (group 3) could not prevent the kidneys from the pathogenic effect of diabetic environment. As shown in Figure 6C(c)) mononuclear cells (**M**) infiltration, and renal corpuscle expansion were observed. A marked collagen (**C**) deposition, and fibrosis (**F**) are shown in Figure 6D(c). In individual treatment with rutin (groups 4), and kaempferol (group 5) (Figure 6C (d, and e)), mesangial expansion was seen, with tubular dilatation, and infiltration, while Figure 6C(f) depicts normal morphology (thymoquinone alone; group 6). This further evident from Figure 6D (d, and e), collagen deposition was more pronounced in group 4, and also seen in group 5. Figure 6D(g) shows lesser or no collagen deposition in group 6. Remarkably, IQ-RKT treatment (group 7) exhibited a robust protective effect, as intact physiological architecture of nephron was observed in Figure 6C(g). Further, Masson's trichrome staining also indicates that IQ-RKT treatment prevented the collagen deposition, and fibrosis (Figure 6D(g)). These findings suggest that IQ-RKT

has the capability to prevent the heart, and kidney from the pathogenic influence of diabetic environment.

The H&E staining of pancreatic specimens from control (group 2) and treatment groups (groups 3-7) shows shrinkage in the size of islets of Langerhans (**IL**), and no mononuclear cells infiltration (Figure 6E (b-f)). These findings indicate that a single dose (45 mg/kg) of STZ to experimental rats is sufficient to produce characteristic signs of chemically induced type 1 diabetes. Moreover, some adipose tissues (**AP**) deposition was also observed, as compared to non-diabetic control (group 1) (Figure 6E(a) where normal islets size, and no adipose tissue deposition was seen.

IQ-RKT Attenuates AGEs induced cardiomyocytes death *via* downregulating RAGE, and TRAF3IP2 protein levels

AGEs induce cardiomyocytes death *via* RAGE[54], and its expression increases the cardiac injury[10]. According to previous studies, RAGE signaling is associated with NOX-mediated ROS generation[55], and TRAF3IP2 activation[10]. TRAF3IP2 is a redox sensitive responsive intermediate, implicated in cardiomyocytes death[10]. We determined the protein levels of RAGE, and TRAF3IP2 in H9c2 cells under *in vitro* AGEs rich environment, and further investigated their expression levels in *in vivo* diabetic model. The exposure of H9c2 cells with MGO-, and Glu-AGEs (24 h) increased the RAGE levels by 4-fold, as compared to negative controls (untreated, BSA, and SP600125), as measured by immunocytochemistry (Figures 7A, and 7B). Whereas, pre-treatment of H9c2 cells with IQ-RKT significantly downregulated the MGO-, and Glu-AGEs-stimulated RAGE levels, as mean fluorescence intensity was decreased by 2.3-fold. The SP600125-treated cells also significantly suppressed the AGEs-stimulated RAGE levels by 3-, and 2.5-fold. RAGE expression was also analyzed by immunoblotting, which also showed the suppressive effect of IQ-RKT on RAGE, with 2-fold decease in response to AGEs, as presented in Figure 7C (a, and b) blots, and Figure 7C (c, and d) graphical representation. We then investigated whether increased expression of RAGE after AGEs stimulation also influence TRAF3IP2 expression. The immunoblots, and graphical presentation (Figure 7C (a, and b; and e, and f) exhibited that both AGEs (MGO-, and Glu-AGEs) have notably upregulated (1.5-, and 1.8-fold) the expression of TRAF3IP2 in H9c2 cells after 24 h. Whereas, pre-treatment with IQ-RKT significantly decreased (1.4-, and 1.3-fold) the AGEs-mediated increase of TRAF3IP2, similar to the treatment with inhibitor SP600125 (1.16-, and 1.3-

fold). These results indicate that AGEs may induce the H9c2 cells death *via* RAGE and TRAF3IP2 activation, and these effects could be inhibited by IQ-RKT treatment.

We next studied whether IQ-RKT can also inhibit the expression of RAGE, and TRAF3IP2 in diabetic SD rats. IQ-RKT treatment exhibited a significant reduction of RAGE, and TRAF3IP2 protein levels (Figure 7D (a), and F (a), and Figure 7E (a), and F (a)), in agreement with *in vitro* results. A significant downregulation of RAGE (1.3-fold) (Figure 7D (b), and F (b)), and TRAF3IP2 (1.5-fold) (Figure 7E (b), and F (c)) expression were exhibited by IQ-RKT treatment (group 7), as compared to diabetic control (group 2). Moreover, IQ-RKT showed a remarkable effect among all the treatment alone groups (groups 4-6). This suggest that IQ-RKT has the potential to attenuate the AGEs-induced elevated RAGE, and TRAF3IP2 protein expression in cardiomyocytes.

IQ-RKT Inhibits AGEs induced activation of JNK, AP-1, and NF-κB

We investigated the AGEs role in cardiomyocytes death *via* studying JNK activation. AGEs activate MAPK (p38) pathway[56], which involves a family of serine-threonine protein kinases. The activation of JNK, key subfamilies of MAPK pathways, cause cellular dysfunction, and apoptosis[57]. Whereas, TRAF3IP2 activates NF-κB, and AP-1 in an IKK- and JNK-dependent manner, respectively[58]. Whether IQ-RKT formulation inhibits AGEs-induced activation of JNK, protein expression analysis was carried out in H9c2 cells by immunoblotting. Both MGO-, and Glu-AGEs significantly induced JNK phosphorylation in H9c2 cells (24 h), as compared to negative controls (untreated, BSA, and SP600125-treated cells). This effect was markedly suppressed by pre-treatment with SP600125, and IQ-RKT, as depicted in Figure 8A (a). IQ-RKT significantly inhibited the MGO-AGEs-induced JNK phosphorylation by 1.5-fold, similar to SP600125-pre-treated cells (Figure 8A (b)), whereas 1.4-fold decrease in Glu-AGEs-induced JNK phosphorylation by IQ-RKT pre-treatment (Figure 8A (c)).

Further, MGO-, and Glu-AGEs-induced AP-1 transcription factor activation in H9c2 cells (Figure 8B (a-d)), was quantified *via* high-throughput DNA-binding ELISA assay (TransAM AP-1 kit) using antibodies. This showed accessible epitopes on c-Jun (detects c-Jun phosphorylation at S73, and JunD phosphorylation at S100), c-Fos, FosB, and JunD proteins upon DNA binding. IQ-RKT pre-treatment inhibited the AGEs-mediated AP-1 activation, as significantly as SP600125 pre-treatment. Moreover, immunoblots (Figure 8C (a-c)) results were also found consistent with

high-throughput assay (AP-1 kit). Similar pattern of inhibition was observed with IQ-RKT pre-treatment. Our results indicate that AGEs can induce the cardiomyocytes death *via* JNK-dependent AP-1 activation, while this effect can be reversed by IQ-RKT treatment. Indeed, similar results were obtained from IQ-RKT treatment in diabetic rats. IQ-RKT treatment (group 7) significantly inhibits the c-Jun phosphorylation, as compared to diabetic control (group 2). IQ-RKT also showed a relatively stronger inhibition of c-Jun phosphorylation, as compared to the treatment alone groups 4-6 (Figure 8D (a, and b)), whereas AG treatment (group 3) failed to inhibit c-Jun activation.

The NF-κB/Rel, a key regulators of cardiomyocytes survival or death, depends on the stimuli[59]. We further investigated whether selective activation of diverse NF-κB/Rel family members by AGEs (MGO-, and Glu-AGEs) might activate the NF-κB signaling in cardiomyocytes. Therefore, the activation state of key transcription activation NF-κB subunits, p65/RelA, and c-Rel, were analyzed by DNA-binding ELISA assay (TransAM NF-κB kit) in H9c2 cells. MGO-, and Glu-AGEs-treated cells showed a significant activation of p65 subunit by 1.6-, and 2.18-fold, as compared to negative controls (untreated cells, BSA, PDTC, and SP600125) (Figure 8E (a)). On the other hand, c-Rel subunit activation was 3.03-, and 1.59-fold (Figure 8E (b) in MGO-, and Glu-AGEs-treated cells, respectively. The NF-κB inhibitor: PDTC, and SP600125 (JNK inhibitor), significantly inhibited the MGO-AGEs-induced p65, and c-Rel activation, while some inhibition was observed against Glu-AGEs. This indicates that AGEs can also induce cardiomyocytes death through NF-κB activation *via* JNK pathway. Whereas, this pro-apoptotic effect of MGO-, and Glu-AGEs was apparently reversed by IQ-RKT pre-treatment, and a significant p65 inhibition (1.4-, and 2.4-fold, respectively) was observed. IQ-RKT also significantly inhibited the MGO-AGEs-induced c-Rel activation by 1.99-fold, while some inactivation in Glu-AGEs-treated cells was also observed. Similarly, IQ-RKT significantly lowered the expression of p65 (Ac-RelA (lys310)) in diabetic rats (group 7) by 2.3-fold, as compared to diabetic control (group 2) (Figure 8F (a, and b)). This further validated our *in vitro* results. Interestingly, AG treatment (group 3) did not cause any inhibition of p65 (Ac-RelA (lys310)). Our results indicate that IQ-RKT has the potential to suppress the AGEs-induced JNK-dependent AP-1/ NF-κB activation.

IQ-RKT Inhibits AGEs mediated pro-apoptotic Bax expression, and increased anti-apoptotic Bcl-2 expression

We further investigated whether IQ-RKT can tilt the balance towards anti-apoptotic state by diminishing AGEs-induced pro-apoptotic Bax (Bcl-2-associated X protein) expression, and increasing anti-apoptotic Bcl-2 (B-cell lymphoma/leukemia 2) expression. Under stress conditions, Bax dissociates from cytoplasmic 14-3-3 proteins, translocates to mitochondria, and release cytochrome c by permeabilizing the outer mitochondrial membrane[60]. MGO-, and Glu-AGEs induced Bax expression has significantly increased in H9c2 cells (Figure 9A (a, and b)), whereas this effect significantly reversed by pre-treatment with SP600125, and IQ-RKT. This indicates that AGEs induce the pro-apoptotic signaling in cardiomyocytes *via* JNK, which up-regulates Bax activity. Similarly, in diabetic rats (group 2), a significant increase in Bax expression was observed, as compared to untreated nondiabetic control (group 1) (Figure 9B (a, and b)). IQ-RKT treatment (group 7) significantly suppressed the Bax levels, as compared to treatment alone groups 4-6. While, AG-treated rats (group 3) also showed a relatively lower production to some extent. Further, Bcl-2 expression was suppressed by AGEs-treatment in H9c2 cells (Figure 9C (a, and b). While, pre-treatment of cells with SP600125, and IQ-RKT had significantly reversed the AGEs-induced Bcl-2 suppressive effect. This finding was also validated in diabetic rats model. IQ-RKT treatment (group 7) significantly increased the expression of Bcl-2 in diabetic rats, as compared to diabetic rats (group 2) (Figure 9D (a, and b). AG-treatment (group 3) was ineffective in elevating the Bcl-2 expression *in vivo*. These results further establish that IQ-RKT can protect cardiomyocytes under stress environment by titling the balance towards anti-apoptotic state through various biochemical mechanisms.

IQ-RKT Inhibits AGEs induced executioner caspase-3 activation in cardiomyocytes

To further investigate the cardioprotective effect of IQ-RKT in reversing the pro-apoptotic effect of AGEs on H9c2 cells[61], we measured the caspase-3/-7 activation levels. As activation of executioner caspases- 3, and -7 prepare cells for apoptosis[62], therefore, activated caspase-3/-7 were first detected in live , as well as in fixed H9c2 cells to predict the mechanism by which IQ-RKT exerts its effect. As depicted in time course curve (Figure 10A), the green fluorescence intensity signals (indicator of caspase-3/-7 activation) was markedly increased in camptothecin

(CPT, apoptosis indicator), and MGO-, and Glu-AGEs-treated cells at 4 h, as compared to untreated, BSA, and SP600125 controls. While a time dependent decrease in the signals intensity was observed in each treatment group. Therefore, 4 h treatment with the stimulants (CPT, and MGO-, and Glu-AGEs) was considered optimal. Pre-treatment with IQ-RKT significantly decreased both the AGEs-mediated activation levels of caspase-3/-7 in live cells (Figure 10B), particularly in MGO-AGEs-treated cells, to a level of negative controls. The caspase-3 and-7 levels in IQ-RKT cells was also relatively reduced than SP600125-treated cells. The qualitative analysis further depicted a significant decrease in AGEs-induced caspase-3 and-7 levels in IQ-RKT cells (Figure 10C, merged), (Figure S7), as compared to CPT, and AGEs-treated controls. *In vivo* studies in diabetic rats further validated our *in vitro* findings. Immunoblot, and its graph (Figure 10D (a, and b)), depict IQ-RKT treatment (group 7) significantly lowered the active caspase-3 protein expression, as compared to diabetic control (group 2). The treatment alone groups 4-5 also showed a significant decrease in the expression of active caspase-3, except group 6, while AG group (group 3) exhibited a weak suppression. These results indicate that IQ-RKT can exert a potent anti-apoptotic effect on cardiomyocytes through suppression of executioner caspase-3 activation.

IQ-RKT improves glucose metabolism with no hypoglycemic effect in non-diabetic rats

We also studied the effect of IQ-RKT on glucose metabolism, and for the treatment-associated hypoglycemia by oral glucose tolerance test (2 g/kg, orally) in healthy non diabetic SD rats. Here, metformin was used as a standard drug. The glucose utilization was enhanced upon treatment with IQ-RKT (group IV), as like controls; untreated (group I), and metformin (group II) groups. In IQ-RKT group, the blood glucose levels reached to a peak at 30 min at 50 mg/kg dose (Figure 11D), as in untreated control (Figure 11A), while at 10, and 100 mg/kg, the peak level was attained at 60 min. After 30 - 60 min, glucose levels curve starts declining, and returned to its basal level after 120 min. This reflects IQ-RKT improved the glucose metabolism. In contrast, in metformin group II, peaked glucose levels remained high between 30 – 60 min at 10-50 mg/Kg, then starts returning to basal levels (Figure 11B). In AG group III, glucose levels peaked at 60 min (Figure 11C), and could not achieve the basal levels even at 120 min. No hypoglycemic activity was observed with IQ-RKT treatment at 10, 50, and 100 mg/kg in healthy non-diabetic rats. Our

results thus indicate that IQ-RKT can improve the glucose metabolism threshold in normal rats with no apparent hypoglycemic effect.

IQ-RKT Overcomes the challenge of stability and intermolecular interactions

The multicomponent natural products formulation often face stability and intermolecular interaction issues[63]. To avoid this is a pre-requisite for their admissibility pharmaceutical product[64]. To assess these parameters, ultraviolet-visible (UV-vis) spectrophotometry was used to evaluate the effect of pH and temperature on the stability of IQ-RKT. Uv-vis spectrophotometry revealed no shift changes in the absorbance of IQ-RKT formulation at pH ranges between 2 to 10 (Figure 12A). The formulation was also found stable up to 50° C (Figure 12B), as no changes were observed in the UV-vis absorbance at 25, 37, 40, and 50° C.

Furthermore, ^{1}H-NMR spectroscopy was employed to study non-covalent interaction among the three components of IQ-RKT. The ^{1}H-NMR of formulation, and each individual natural product (rutin, kaempferol, and thymoquinone) were recorded with tetramethylsilane (TMS), as an internal standard (Figure 12C). The result showed no chemical shift changes in IQ-RKT formulation spectrum, as compared to spectra of individual component. This further supported the stability of a multicomponent natural formulation.

DISCUSSION

Cardiovascular diseases (CVDs) are the key cause of mortality in patients with diabetes[65]. Cardiac tissue dysfunction is associated with AGEs, which is a significant factor for non-ischemic CVD[66]. Whereas AOPPs a risk factor for IHD[10]. AGEs cause the cardiac tissue dysfunction *via* a combination of direct structural alteration, and receptor-stimulated oxidative stress, and inflammatory responses. This ultimately leads to coronary artery disease, and heart failure[67]. It has been reported that apoptosis is involved in the pathogenesis of almost all heart diseases, such as ischemia-associated ailments, including acute and chronic stages of myocardial infarction, ischemia-reperfusion, cardiomyopathy, and hibernating myocardium. Other ailments, including dilated cardiomyopathy, are also associated with cardiomyocytes apoptosis[68]. However, no in-depth mechanistic study was conducted to understand the role of AGEs in cardiomyocytes apoptosis, and thus on therapeutic interventions to address this issue. In the

current study, we studied the role of AGEs in cardiomyocytes injury both *in vitro,* and *in vivo* diabetic environment. As a result, we identified a mechanism of AGEs-RAGE-ROS-dependent TRAF3IP2/JNK associated pro-apoptotic pathway in H9c2 cells, and heart tissues of diabetic rats. Further, a formulation IQ-RKT, comprised of three natural ingredients (rutin, kaempferol, and thymoquinone), was developed to ameliorate the AGEs-induced cardiomyocytes death *via* downregulating the TRAF3IP2/JNK-dependent AP-1/ NF-κB activation.

Medicinal plants have been used for the treatment of cardiovascular diseases since antiquity[69], therefore, bioactive plant metabolites, rutin[70], kaempferol[71], and thymoquinone[72], were carefully selected, based on their reported antioxidant, anti-inflammatory, and cardioprotective properties, to study in combination (IQ-RKT) their potential to suppress the AGEs-mediated cardiomyocytes death. Our results show that AGEs induce H9c2 cells death, and similar effect were observed in *in vivo* type 1 diabetic SD rats heart tissues, with elevated expression of RAGE. RAGE is the most important receptor for AGEs, and expressed on many cell types, including cardiac myocytes, endothelial cells, macrophages, and monocytes. The activation of RAGE increased RAGE expression itself, creating a viscous cycle that intensifies and perpetuates AGEs associated intracellular oxidative stress, and inflammatory response[67]. We found that the AGE-RAGE axis results in intracellular oxidative stress, and TRAF3IP2 activation. This leads to AP-1/ NF-κB transactivation *via* JNK activation. Besides, AGEs-induce Bax expression, resulting in cytochrome-c release, and caspase-3 activation. In addition, AGEs suppress the anti-apoptotic Bcl-2 protein expression. These results demonstrated that AGEs can induce cardiomyocytes death by causing the activation of pro-apoptotic pathway *via* RAGE-mediated signaling nexus, whereas treatment with the newly developed formulation IQ-RKT reversed this effect, both *in vitro*, and *in vivo*. IQ-RKT apparently exerted cardioprotective effect independent of hyperglycemic milieu, as no suppressive effect was observed on FBG, and HbA1c (Amadori product) in diabetic SD rats. The heart tissue injury was also observed in diabetic SD rats, along with elevated levels of plasma cardiac injury markers, such as LDH, CK-MB, and cTnI. Histopathological examination further established heart, and kidney tissues injury under diabetic environment. The kidney serves as a major site of AGEs clearance, and there is a positive correlation between chronic kidney diseases, and circulating AGEs levels[73,74]. We found that IQ-

772 RKT treatment to diabetic rats prevented the kidney tissue from diabetic insults, which might
773 have resulted in lowering the plasma AGEs levels. Whereas, AG-treated diabetic rats have shown
774 marked sign of kidney damage, and mononuclear cells infiltration, a typical feature of type-1
775 diabetes in experimental rats. This also leads to further weight reduction in AG diabetic rats.

776 The systemic levels of AGEs increase in diabetes[75], along with AOPPs levels. This cause an early
777 onset of atherosclerosis, chronic kidney disease, and coronary artery diseases, and in diabetes
778 mellitus[76-78]. Our study on diabetic SD rats, spread over 12 weeks, also showed increased plasma
779 levels of glycooxidative stress markers, including protein carbonyl stress markers, TBARS levels,
780 AOPPs, and AGEs levels. Whereas IQ-RKT treatment remarkably ameliorated glycooxidative
781 stress marker levels. We observed that H9c2 cells, upon stimulation by MGO-, and Glu-AGEs
782 showed an increased expression of RAGE, and associated ROS generation. Similar effect of AGEs
783 accumulation in cardiac tissue was observed in *in vivo* diabetic rats. *RAGE* gene is responsive to
784 oxidative stress. *RAGE* gene promotors include redox-sensitive transcription factors binding sites,
785 such as AP-1, NF-κB, and Sp1[79]. RAGE expression also increases in the conditions, such as
786 diabetes, cardiovascular diseases, and chronic inflammation[80,81]. It has been reported that
787 targeting *RAGE* gene or its expression suppressed the cardiac injury[80,81]. Interestingly IQ-RKT
788 treatment lowered the AGEs-mediated increased expression of RAGE in H9c2 cells, as well as in
789 the heart tissues of experimental rats. The formulation IQ-RKT not only suppressed the AGEs-
790 induced intracellular oxidative stress, but also downregulated the redox sensitive TRAF3IP2
791 activation, and associated cardiomyocytes apoptosis. Thus, RAGE-TRAF3IP2 signaling may serve
792 as a therapeutic target for the treatment of cardiovascular disease. The study by Valente *et.al*.
793 also in line with our findings that attenuation of RAGE blocks the TRAF3IP2-mediated cardiac
794 injury[10].

795 Our study also showed that AGE-RAGE nexus involves JNK pathway in cardiomyocytes, as JNK
796 inhibitor (SP600125) was found effective in suppressing AGEs-induced cardiomyocytes death.
797 The MAPK (mitogen-activated protein kinase) signaling pathway, particularly JNK and p38, is
798 collectively termed as stress-activated protein kinases. It contributes to myocytes apoptosis, and
799 heart diseaeses[82]. IQ-RKT treatment noticeably inhibited the AGEs-mediated JNK signaling, and
800 hence prevented the cardiomyocytes apoptosis *in vitro*.

We found that AGEs are key cause of the transactivation of AP-1 (c-Jun, c-Fos, FosB, and JunD), and NF-κB (p65) and c-Rel) subunits *via* RAGE/ROS/TRAF3IP2/JNK pathway. As their inhibition were observed in H9c2 cells through SP600125 (JNK inhibitor), and PDTC (NF-κB inhibitor), which further supported our findings. IQ-RKT formulation suppressed the transactivation of both redox-sensitive transcription factors. In cardiomyocytes, RelA/c-Rel transactivation generally leads to pro-apoptotic gene activation, where c-Rel particularly exhibits a prominent role in heart remodeling and hypertrophy[83,84]. Many stress stimuli are able to induce activation of AP-1 protein, and hence lead to cardiomyocytes death[10,85.] Our study demonstrated that IQ-RKT inhibits AP-1/NF-κB activation *via* JNK pathway, and thus prevents the AGEs-induced cardiomyocytes apoptosis.

The Bcl-2 family, comprising of pro-apoptotic (Bax, Bad, and Bim), and anti-apoptotic (Bcl-2, and Bcl-xL) proteins, is an important regulator of cell survival, and death[10]. The pathogenesis of myocardial infarction and heart failure are directly linked to apoptosis[86]. Here in our study we showed that AGEs can shift the balance towards pro-apoptotic pathway, causing the activation of Bax *via* JNK pathway, and thus raising cytoplasmic cytochrome c levels. This leads to the activation of key executioner protein, caspase-3 in H9c2 cells *in vitro*, and in the heart tissue *in vivo*. Whereas standard SP600125 inhibited the AGEs-induced Bax activation, and up-regulated the Bcl-2 expression. IQ-RKT formulation protected the cardiomyocytes by decreasing the AGEs-mediated Bax activation, decreased cytoplasmic cytochrome c levels, downregulated caspase-3 activation, and increased the Bcl-2 activation. Collectively IQ-RKT tilted the balance towards an anti-apoptotic pathway (Figure 13).

The IQ-RKT formulation also found stable at different pH and temperature range, as checked by Uv-vis spectrophotometry. Furthermore, intermolecular interactions among its components, *i.e.*, rutin, kaempferol, and thymoquinone, were not significant. This made IQ-RKT a candidate formulation for further pre-clinical and clinical trials. Moreover, IQ-RKT significantly enhanced the glucose tolerance in non-diabetic rats, without causing a hypoglycemia.

CONCLUSION

In this study, we analyzed the role of AGEs in cardiomyocytes apoptosis in *in vitro* H9c2 cells, as well as in *in vivo* diabetic rats-based model. Through this approach, we identified that AGE-RAGE axis is associated with cardiomyocytes death *via* ROS-dependent TRAF3IP2/JNK-activated NF-κB/AP1 pathway. Therefore, by targeting this pathway, a natural product-based antiglycation formulation IQ-RKT, comprise of rutin, kaempferol, and thymoquinone, tilted the balance towards anti-apoptosis, and exhibited cardioprotective effect. These findings provide a strong basis to study IQ-RKT through clinical trial against diabetic cardiac injury, and other cardiovascular complications.

ACKNOWLEDGEMENTS

This study was funded by the World Bank supported Grand Challenge Funds (Grant No: 20-GCF-1044/RGM/R&ID/HEC/2021) (Higher Education Commission) to Prof. M. Iqbal Choudhary after a nation-wide competition. We acknowledge the staff of National Facility for Laboratory Animal Research and Care (NFLARC), ICCBS, for their help in animal handling.

DECLARATION OF INTERESTS

The authors declare no competing interests.

AUTHORS CONTRIBUTIONS

Conceptualization, M. Iqbal Choudhary, and Humera Jahan; methodology, M. Iqbal Choudhary, Humera Jahan, Urooba Fatima, and Sana Asad; investigation M. Iqbal Choudhary, and Humera Jahan; art work, M. Iqbal Choudhary, Humera Jahan, Urooba Fatima, Sana Asad , Sidra Zahoor, Priya Tufail, Dania Zainab, Nimra Naz Siddiqui and Aaqib Ullah; writing – original draft, M. Iqbal Choudhary, and Humera Jahan; writing – review & editing, M. Iqbal Choudhary, Humera Jahan, and Marina Pizzi; funding acquisition, M. Iqbal Choudhary; resources, M. Iqbal Choudhary, and Humera Jahan; supervision, M. Iqbal Choudhary, and Humera Jahan.

REFERENCES

1. Matheus ASdM, Tannus LRM, Cobas RA, Palma CCS, Negrato CA, Gomes MdB. Impact of diabetes on cardiovascular disease: an update. *International Journal of Hypertension*. 2013;2013(1):653789.
2. Association AD. Diabetes Complications-Cardiovascular Disease. https://diabetes.org/about-diabetes/complications/cardiovascular-

disease#:~:text=Of%20diabetes%20complications%2C%20this%20is,people%20with%20type%202%20diabetes.
3. Fan W. Epidemiology in diabetes mellitus and cardiovascular disease. *Cardiovascular Endocrinology & Metabolism*. 2017;6(1):8-16.
4. Martín-Timón I, Sevillano-Collantes C, Segura-Galindo A, del Cañizo-Gómez FJ. Type 2 diabetes and cardiovascular disease: have all risk factors the same strength? *World Journal of Diabetes*. 2014;5(4):444.
5. Anwar MMU, Jahan SMS, Afrin S, Hossain MZ. Diabetic and non-diabetic subjects with ischemic stroke: risk factors, stroke topography and hospital outcome. *Journal of Medicine*. 2017;18(2):75.
6. Rösen P, Nawroth P, King G, Möller W, Tritschler HJ, Packer L. The role of oxidative stress in the onset and progression of diabetes and its complications: asummary of a Congress Series sponsored byUNESCO-MCBN, the American Diabetes Association and the German Diabetes Society. *Diabetes/metabolism Research and Reviews*. 2001;17(3):189-212.
7. Kim Y. Blood and tissue advanced glycation end products as determinants of cardiometabolic disorders focusing on human studies. *Nutrients*. 2023;15(8):2002.
8. Cao W, Hou FF, Nie J. AOPPs and the progression of kidney disease. *Kidney International Supplements*. 2014;4(1):102-106.
9. Lee J, Yun J-S, Ko S-H. Advanced glycation end products and their effect on vascular complications in type 2 diabetes mellitus. *Nutrients*. 2022;14(15):3086.
10. Valente AJ, Yoshida T, Clark RA, Delafontaine P, Siebenlist U, Chandrasekar B. Advanced oxidation protein products induce cardiomyocyte death via Nox2/Rac1/superoxide-dependent TRAF3IP2/JNK signaling. *Free Radical Biology and Medicine*. 2013;60:125-135.
11. Rhee SY, Kim YS. The role of advanced glycation end products in diabetic vascular complications. *Diabetes & Metabolism Journal*. 2018;42(3):188-195.
12. Hegab Z, Gibbons S, Neyses L, Mamas MA. Role of advanced glycation end products in cardiovascular disease. *World Journal of Cardiology*. 2012;4(4):90.
13. Jahan H, Siddiqui NN, Iqbal S, et al. Indole-linked 1, 2, 3-triazole derivatives efficiently modulate COX-2 protein and PGE2 levels in human THP-1 monocytes by suppressing AGE-ROS-NF-kβ nexus. *Life Sciences*. 2022;291:120282.
14. Gutierrez SH, Kuri MR, del Castillo ER. Cardiac role of the transcription factor NF-κB. *Cardiovascular & Haematological Disorders-Drug Targets (Formerly Current Drug Targets-Cardiovascular & Hematological Disorders)*. 2008;8(2):153-160.
15. Yoshida T, Das NA, Carpenter AJ, et al. Minocycline reverses IL-17A/TRAF3IP2-mediated p38 MAPK/NF-κB/iNOS/NO-dependent cardiomyocyte contractile depression and death. *Cellular signalling*. 2020;73:109690.
16. Das NA, Carpenter AJ, Yoshida T, et al. TRAF3IP2 mediates TWEAK/TWEAKR-induced pro-fibrotic responses in cultured cardiac fibroblasts and the heart. *Journal of Molecular and Cellular Cardiology*. 2018;121:107-123.
17. Liao Y-H, Xia N, Zhou S-F, et al. Interleukin-17A contributes to myocardial ischemia/reperfusion injury by regulating cardiomyocyte apoptosis and neutrophil infiltration. *Journal of the American College of Cardiology*. 2012;59(4):420-429.
18. Wei J, Yan T, Liang YJDDR. Targeting TRAF3IP2 alleviates high glucose-induced cardiomyocyte inflammation and apoptosis. *Drug Development Research*. 2022;83(1):167-175.
19. Wang Y, Ping LF, Bai FY, Zhang XH, Li GHJI, Inflammation, Disease. Hmgcs2 is the hub gene in diabetic cardiomyopathy and is negatively regulated by Hmgcs2, promoting high glucose-induced cardiomyocyte injury. *Immunity, Inflammation and Disease*. 2024;12(3):e1191.
20. Schalkwijk C, Stehouwer C. Methylglyoxal, a highly reactive dicarbonyl compound, in diabetes, its vascular complications, and other age-related diseases. *Physiological Reviews*. 2020;100(1):407-461.

21. Dias MC, Pinto DC, Silva AM. Plant flavonoids: Chemical characteristics and biological activity. *Molecules*. 2021;26(17):5377.
22. Ullah A, Munir S, Badshah SL, et al. Important flavonoids and their role as a therapeutic agent. *Molecules*. 2020;25(22):5243.
23. Chen X, Yu M, Xu W, et al. Rutin inhibited the advanced glycation end products-stimulated inflammatory response and extra-cellular matrix degeneration *via* targeting TRAF-6 and BCL-2 proteins in mouse model of osteoarthritis. *Aging (albany NY)*. 2021;13(18):22134.
24. Liga S, Paul C, Péter F. Flavonoids: Overview of biosynthesis, biological activity, and current extraction techniques. *Plants*. 2023;12(14):2732.
25. Dandawate PR, Vyas AC, Padhye SB, Singh MW, Baruah JB. Perspectives on medicinal properties of benzoquinone compounds. *Mini Reviews in Medicinal Chemistry*. 2010;10(5):436-454.
26. Sethi G, Ahn KS, Aggarwal BB. Targeting nuclear factor-κB activation pathway by thymoquinone: role in suppression of antiapoptotic gene products and enhancement of apoptosis. *Molecular cancer research*. 2008;6(6):1059-1070.
27. Witek P, Korga A, Burdan F, et al. The effect of a number of H9c2 rat cardiomyocytes passage on repeatability of cytotoxicity study results. *Cytotechnology*. 2016;68(6):2407-2415.
28. Jahan H, Siddiqui NN, Iqbal S, et al. Suppression of COX-2/PGE2 levels by carbazole-linked triazoles via modulating methylglyoxal-AGEs and glucose-AGEs–induced ROS/NF-κB signaling in monocytes. *Cellular Signalling*. 2022;97:110372.
29. Jahan H, Choudhary MI. Gliclazide alters macrophages polarization state in diabetic atherosclerosis in vitro via blocking AGE-RAGE/TLR4-reactive oxygen species-activated NF-kβ nexus. *European Journal of Pharmacology*. 2021;894:173874.
30. Jahan H, Choudhary MI, Manzoor M, Khan KM, Perveen S. Insulinotropic action of 2, 4-dinitroanilino-benzoic acid through the attenuation of pancreatic beta-cell lesions in diabetic rats. *Chemico-Biological Interactions*. 2017;273:237-244.
31. Lima TFO, Costa MC, Figueiredo ID, et al. Curcumin, Alone or in Combination With Aminoguanidine, Increases Antioxidant Defenses and Glycation Product Detoxification in Streptozotocin-Diabetic Rats: A Therapeutic Strategy to Mitigate Glycoxidative Stress. *Oxidative medicine and cellular longevity*. 2020;2020(1):1036360.
32. Ihm S-H, Yoo HJ, Park SW, Ihm J. Effect of aminoguanidine on lipid peroxidation in streptozotocin-induced diabetic rats. *Metabolism*. 1999;48(9):1141-1145.
33. de Vos LC, Lefrandt JD, Dullaart RP, Zeebregts CJ, Smit AJ. Advanced glycation end products: An emerging biomarker for adverse outcome in patients with peripheral artery disease. *Atherosclerosis*. 2016;254:291-299.
34. Wu Q, Zhong Z-M, Pan Y, et al. Advanced oxidation protein products as a novel marker of oxidative stress in postmenopausal osteoporosis. *Medical Science Monitor: International Medical Journal of Experimental and Clinical Research*. 2015;21:2428.
35. I. Lindberg JRP. *Molecular Cell Biology, Chapter in Encyclopedia of Cell Biology*. 2016.
36. Gaweł S, Wardas M, Niedworok E, Wardas P. Malondialdehyde (MDA) as a lipid peroxidation marker. *Wiadomosci lekarskie (Warsaw, Poland: 1960)*. 2004;57(9-10):453-455.
37. (2021). KKG. Emergency MedicineCardiac Markers. https://emedicine.medscape.com/article/811905-overview?form=fpf
38. Hernández-Morera P, Castaño-González I, Travieso-González CM, Mompeó-Corredera B, Ortega-Santana F. Quantification and statistical analysis methods for vessel wall components from stained images with Masson's trichrome. *PloS one*. 2016;11(1):e0146954.
39. Jahan H, Tufail P, Shamim S, et al. 1, 2, 4-Triazine derivatives as agents for the prevention of AGE-RAGE-mediated inflammatory cascade in THP-1 monocytes: An approach to prevent inflammation-induced late diabetic complications. *International Immunopharmacology*. 2024;142:113145.

40. Carter LG, Qi NR, De Cabo R, Pearson KJ. Maternal exercise improves insulin sensitivity in mature rat offspring. *Medicine and Science in Sports and Exercise*. 2013;45(5):832.
41. Li P, Nijhawan D, Budihardjo I, et al. Cytochrome c and dATP-dependent formation of Apaf-1/caspase-9 complex initiates an apoptotic protease cascade. *Cell*. 1997;91(4):479-489.
42. Goldstein J, Munoz-Pinedo C, Ricci J, et al. Cytochrome c is released in a single step during apoptosis. *Cell Death & Differentiation*. 2005;12(5):453-462.
43. Thornalley PJ. Use of aminoguanidine (Pimagedine) to prevent the formation of advanced glycation endproducts. *Archives of Biochemistry and Biophysics*. 2003;419(1):31-40.
44. Soulis T, Cooper ME, Sastra S, et al. Relative contributions of advanced glycation and nitric oxide synthase inhibition to aminoguanidine-mediated renoprotection in diabetic rats. *Diabetologia*. 1997;40:1141-1151.
45. Veeresh B Hubballi NBH, Shruthi K R, Avinash, Anshu Kumar Yadav, Anil Kumar K M, Jeyaprakash M R, Chethan kumar B G. The Study of Comparison between HbA1c% and Glycated Albumin % in Diabetic ESRD Patients on MHD. *Journal of Carcinogenesis*. 2025;24(2s):1342-1348.
46. Hegab Z, Gibbons S, Mohamed T, et al. 010 Advanced glycation end products induce functional impairment in neonatal rat cardiomyocytes through enhanced production of reactive oxygen species. *Heart* 2010;96:A9-A10.
47. Cepas V, Collino M, Mayo JC, Sainz RM. Redox signaling and advanced glycation endproducts (AGEs) in diet-related diseases. *Antioxidants*. 2020;9(2):142.
48. Faria A, Persaud SJ. Cardiac oxidative stress in diabetes: mechanisms and therapeutic potential. *Pharmacology & Therapeutics*. 2017;172:50-62.
49. Mohamed J, Shing SW, Idris MHM, Budin SB, Zainalabidin S. The protective effect of aqueous extracts of roselle (Hibiscus sabdariffa L. UKMR-2) against red blood cell membrane oxidative stress in rats with streptozotocin-induced diabetes. *Clinics*. 2013;68(10):1358-1363.
50. Krawczyk M, Burzynska-Pedziwiatr I, Wozniak LA, Bukowiecka-Matusiak M. Impact of polyphenols on inflammatory and oxidative stress factors in diabetes mellitus: nutritional antioxidants and their application in improving antidiabetic therapy. *Biomolecules*. 2023;13(9):1402.
51. Nowotny K, Jung T, Höhn A, Weber D, Grune T. Advanced glycation end products and oxidative stress in type 2 diabetes mellitus. *Biomolecules*. 2015;5(1):194-222.
52. De Geest B, Mishra M. Role of oxidative stress in diabetic cardiomyopathy. *Antioxidants*. 2022;11(4):784.
53. Zhang H, Kang K, Chen S, et al. High serum lactate dehydrogenase as a predictor of cardiac insufficiency at follow-up in elderly patients with acute myocardial infarction. *Archives of Gerontology and Geriatrics*. 2024;117:105253.
54. Zhao G, Zhang X, Wang H, Chen Z. Beta carotene protects H9c2 cardiomyocytes from advanced glycation end product-induced endoplasmic reticulum stress, apoptosis, and autophagy via the PI3K/Akt/mTOR signaling pathway. *Annals of Translational Medicine*. 2020;8(10)
55. Shanmugam P, Valente AJ, Prabhu SD, et al. Angiotensin-II type 1 receptor and NOX2 mediate TCF/LEF and CREB dependent WISP1 induction and cardiomyocyte hypertrophy. *Journal of Molecular and Cellular Cardiology*. 2011;50(6):928-938.
56. Chang P-C, Chen T-H, Chang C-J, Hou C-C, Chan P, Lee H-M. Advanced glycosylation end products induce inducible nitric oxide synthase (iNOS) expression via a p38 MAPK-dependent pathway. *Kidney International*. 2004;65(5):1664-1675.
57. Chen J, Jing J, Yu S, et al. Advanced glycation endproducts induce apoptosis of endothelial progenitor cells by activating receptor RAGE and NADPH oxidase/JNK signaling axis. *American Journal of Translational Research*. 2016;8(5):2169.

58. Valente AJ, Clark RA, Siddesha JM, Siebenlist U, Chandrasekar B. CIKS (Act1 or TRAF3IP2) mediates Angiotensin-II-induced Interleukin-18 expression, and Nox2-dependent cardiomyocyte hypertrophy. *Journal of Molecular and Cellular Cardiology*. 2012;53(1):113-124.
59. Valen G, Yan Z-q, Hansson GK. Nuclear factor kappa-B and the heart. *Journal of the American College of Cardiology*. 2001;38(2):307-314.
60. Tsuruta F, Sunayama J, Mori Y, et al. JNK promotes Bax translocation to mitochondria through phosphorylation of 14-3-3 proteins. *The EMBO Journal*. 2004;23(8):1889-1899.
61. Li Y-H, Zhang W-L, Zhou H-Y, Yu D-W, Sun X-N, Hu Q. Halofuginone protects against advanced glycation end products-induced injury of H9C2 cells via alleviating endoplasmic reticulum stress-associated apoptosis and inducing autophagy. *Molecular Medicine Reports*. 2019;20(4):3131-3139.
62. van Empel VP, Bertrand AT, Hofstra L, Crijns HJ, Doevendans PA, De Windt LJ. Myocyte apoptosis in heart failure. *Cardiovascular Research*. 2005;67(1):21-29.
63. Thakur L, Ghodasra U, Patel N, Dabhi M. Novel approaches for stability improvement in natural medicines. *Pharmacognosy Reviews*. 2011;5(9):48.
64. Bajaj S, Singla D, Sakhuja N. Stability testing of pharmaceutical products. *Journal of Applied Pharmaceutical Science*. 2012;(Issue):129-138.
65. Ma C-X, Ma X-N, Guan C-H, Li Y-D, Mauricio D, Fu S-B. Cardiovascular disease in type 2 diabetes mellitus: progress toward personalized management. *Cardiovascular Diabetology*. 2022;21(1):74.
66. Takata T, Inoue S, Masauji T, Miyazawa K, Motoo Y. Generation and accumulation of various advanced glycation end-products in cardiomyocytes may induce cardiovascular disease. *International Journal of Molecular Sciences*. 2024;25(13):7319.
67. Hartog JW, Voors AA, Bakker SJ, Smit AJ, van Veldhuisen DJ. Advanced glycation end-products (AGEs) and heart failure: pathophysiology and clinical implications. *European Journal of Heart Failure*. 2007;9(12):1146-1155.
68. Takemura G, Fujiwara H. Morphological aspects of apoptosis in heart diseases. *Journal of Cellular and Molecular Medicine*. 2006;10(1):56-75.
69. Chang X, Zhang T, Zhang W, Zhao Z, Sun J. Natural drugs as a treatment strategy for cardiovascular disease through the regulation of oxidative stress. *Oxidative Medicine and Cellular Longevity*. 2020;2020(1):5430407.
70. Prasad R, Prasad SB. A review on the chemistry and biological properties of Rutin, a promising nutraceutical agent. *Asian J Pharm Pharmacol*. 2019;5(1):1-20.
71. Gutiérrez-del-Río I, Villar CJ, Lombó F. Therapeutic uses of kaempferol: Anticancer and antiinflammatory activity. *Biosynthesis, Food Sources and Therapeutic Uses*. 2016;15(2):71.
72. Zari A, Zari TA. Antioxidant, anti-Inflammatory and anticancer activities of thymoquinone: A review. *Word Appl Sci J*. 2020;38:250-263.
73. Fotheringham AK, Gallo LA, Borg DJ, Forbes JM. Advanced glycation end products (AGEs) and chronic kidney disease: does the modern diet AGE the kidney? *Nutrients*. 2022;14(13):2675.
74. Prasad C, Davis KE, Imrhan V, Juma S, Vijayagopal P. Advanced glycation end products and risks for chronic diseases: intervening through lifestyle modification. *American Journal of Lifestyle Medicine*. 2019;13(4):384-404.
75. Zawada A, Machowiak A, Rychter AM, et al. Accumulation of advanced glycation end-products in the body and dietary habits. *Nutrients*. 2022;14(19):3982.
76. Sorescu D, Weiss D, Lassègue B, et al. Superoxide production and expression of nox family proteins in human atherosclerosis. *Circulation*. 2002;105(12):1429-1435.
77. Brownlee M. Biochemistry and molecular cell biology of diabetic complications. *Nature*. 2001;414(6865):813-820.
78. Kaneda H, Taguchi J, Ogasawara K, Aizawa T, Ohno M. Increased level of advanced oxidation protein products in patients with coronary artery disease. *Atherosclerosis*. 2002;162(1):221-225.

79. Li J, Qu X, Schmidt AM. Sp1-binding elements in the promoter of RAGE are essential for amphoterin-mediated gene expression in cultured neuroblastoma cells. *Journal of Biological Chemistry*. 1998;273(47):30870-30878.
80. Ong S-B, Hernández-Reséndiz S, Crespo-Avilan GE, et al. Inflammation following acute myocardial infarction: multiple players, dynamic roles, and novel therapeutic opportunities. *Pharmacology & Therapeutics*. 2018;186:73-87.
81. Bucciarelli LG, Kaneko M, Ananthakrishnan R, et al. Receptor for advanced-glycation end products: key modulator of myocardial ischemic injury. *Circulation*. 2006;113(9):1226-1234.
82. Wang Y, Su B, Sah VP, Brown JH, Han J, Chien KR. Cardiac hypertrophy induced by mitogen-activated protein kinase kinase 7, a specific activator for c-Jun NH2-terminal kinase in ventricular muscle cells. *Journal of Biological Chemistry*. 1998;273(10):5423-5426.
83. Gaspar-Pereira S, Fullard N, Townsend PA, et al. The NF-κB subunit c-Rel stimulates cardiac hypertrophy and fibrosis. *The American Journal of Pathology*. 2012;180(3):929-939.
84. Hunter JE, Leslie J, Perkins ND. c-Rel and its many roles in cancer: an old story with new twists. *British Journal of Cancer*. 2016;114(1):1-6.
85. Maulik N, Goswami S, Galang N, Das DK. Differential regulation of Bcl-2, AP-1 and NF-κB on cardiomyocyte apoptosis during myocardial ischemic stress adaptation. *FEBS Letters*. 1999;443(3):331-336.
86. Garg S, Narula J, Chandrashekhar Y. Apoptosis and heart failure: clinical relevance and therapeutic target. *Journal of Molecular and Cellular Cardiology*. 2005;38(1):73-79.

Figure Captions

Figure 1: Schematic representation of the pre-clinical experimental design.

Schematic diagram illustrating *in vitro*- and *in vivo* experimental approaches, bioassays, and techniques employed during the study. From the left panel (A) H9c2 embryonic cardiomyocytes were stimulated with pathogenic factors MGO-, and glucose-AGEs in order to induce apoptosis, while the entire cascade was reversed by the treatment with IQ-RKT formulation, a newly developed natural product-based formulation. The cardioprotective effect of IQ-RKT formulation was validated (B) through *in vivo* study using diabetic SD rats model.

Figure 2: IQ-RKT Prevents *in vitro* AGEs-induced cardiomyocytes death.

(A) Quantitative analysis of AGEs (MGO-, and Glu-AGEs), and IQ-RKT-treatment on the H9c2 cells viability.

(B) Morphological assessment of AGEs-treated H9c2 cells under IQ-RKT pre-treatment.

(C) Quantification of cytochrome c levels in H9c2 cells.

- Formulation IQ-RKT (an equimolar composition of Rutin, Kaempferol, and Thymoquinone)
- The data (A-C) represent the mean ± SD; ∗∗, ##, and σσ $p < 0.01$; ∗∗∗, ###, and σσσ $p < 0.001$. *AGEs *vs*. Control; $^{\#}$IQ-RKT *vs*. MGO-AGEs; $^{\sigma}$IQ-RKT *vs*. Glu-AGEs.

Figure 3: Effect of IQ-RKT on the body weights, and glycemic parameters in STZ-induced diabetic rats.

(A) IQ-RKT showed no significant reduction of body weight in diabetic rats.

(B) IQ-RKT did not affect FBG levels in diabetic rats.

(C) IQ-RKT have no effect on the HbA1c levels in diabetic rats.

(D) IQ-RKT significantly reduced the glycated albumin in diabetic rats.

- ND: Nondiabetic control; D: Diabetic control; AG: Aminoguanidine; R: Rutin; K: Kaempferol; T: Thymoquinone; IQ-RKT: 1/3 composition of Rutin, Kaempferol, and Thymoquinone
- D+AG (50 mg/kg/d); D+R (16.6 mg/kg/d); D+K (16.6 mg/kg/d); D+T (16.6 mg/kg/d); D+ IQ-RKT (50 mg/kg/d).
- The data represents the mean ± SD; ***, ###, ~~~, and ††† $p < 0.001$; ** $p < 0.01$; ns ≤ 0.99; * D *vs*. ND; $^{\#}$ AG, R, K, T, and IQ-RKT *vs*. D; $^{\sim}$ R, K, T, and IQ-RKT *vs*. AG; † IQ-RKT *vs*. R, K, T.

Figure 4: IQ-RKT Inhibits glycooxidative stress in H9c2 cardiomyocytes and diabetic heart.

(A) IQ-RKT treatment inhibited the ROS generation in H9c2 cardiomyocytes.

(B) Oxidative stress analysis through quantification of MDA levels in heart tissues.

(C) Quantitative analysis of protein carbonyl stress in diabetic heart, and treatment groups.

(D) IQ-RKT decreased the plasma AGEs levels in diabetic rats.

(E) (a) Immunostained sections of diabetic heart tissue. Circles indicate the deposition of AGEs. (b) Mean Fluorescence Intensity (MFI) of AGEs, measured by Image J.

(F) (a) Immunoblot expression of AGEs in cardiac tissues. (b) Quantification of AGEs signal.

(G) AOPPs plasma levels in diabetic rats, and treatment groups.

(H) SOD enzyme levels in diabetic heart tissues, and treatment groups.

(I) Catalase enzyme levels in diabetic heart tissues, and treatment groups.

(J) GSH enzyme levels in diabetic heart tissues, and treatment groups.

Figure 5: IQ-RKT Improved the cardiac functions in diabetic rats.

(A) LDH plasma levels in diabetic rats, and treatment groups.

(B) CK-MB plasma levels in diabetic rats, and treatment groups.

(C) cTnI plasma levels in diabetic rats, and treatment groups.

Figure 6: Histological analysis of heart, kidney, and pancreas tissues of diabetic rats after IQ-RKT treatment.

(A) H&E-stained sections of cardiac tissues. BCM: Branched cardiomyocyte, C: Capillary, F: Fibril, ID: Intercalated disc, FB: Fibroblast, BV: Blood vessels, N: Nuclei.
(B) Masson's trichrome stained sections of heart tissues. C: Collagen, F: Fibrosis.
(C) H&E-stained sections of kidney tissues. BC: Bowman's capsule, BS: Bowman's space, G: Glomerulus, PT: Proximal tubule, dT: Distal tubules, N: Nucleus, M: Mononuclear cells, IF: Interstitial fibrosis.
(D) Masson's trichrome stained sections of kidney tissues. F: Fibrosis, C: Collagen.
(E) H&E-stained sections of pancreas tissues. IL: Islets of Langerhans, AP: Adipose tissues.

Figure 7: IQ-RKT Inhibits cardiomyocytes death *via* suppressing RAGE and TRAF3IP2 protein expression.

(A) Immunocytochemical investigation of RAGE (merged) in AGEs-treated H9c2 cells, and pre-treated IQ-RKT cells. Also see separate channels, Texas Red, and DAPI (Figure S4).
(B) MFI of RAGE in H9c2 cells.
(C) (a and b) Immunoblot expression of RAGE and TRAF3IP2 in MGO-, and Glu-AGEs treated, and IQ-RKT H9c2 cells. (c and d) Quantification of RAGE signal. (e and f) Quantification of TRAF3IP2 signal.
(D) (a) Immunohistology of heart tissues of diabetic rats, and treatment groups. Circles indicate elevated RAGE signal. (b) MFI of RAGE levels assessed *via* Image J.
(E) (a) Immunohistology of heart tissues of diabetic rats, and treatment groups. Circles indicate elevated TRAF3IP2 signal. (b) MFI of TRAF3IP2 levels assessed *via* Image J.
(F) (a) Immunoblot expression of TRAF3IP2 and RAGE in heart tissues of diabetic rats, and treatment groups. (b and c) Quantification of TRAF3IP2 and RAGE signals *via* image J software.

Figure 8: IQ-RKT Prevents JNK-dependent AP-1 and NF-kB transactivation in cardiomyocytes.

(A) (a and b) Immunoblot expression of JNK in H9c2 cells under the influence of MGO-, and Glu-AGEs.

(c and d) Quantitative analysis of phospho-JNK signals in MGO-, and Glu-AGEs-treated H9c2 cells.
(B) Effect of IQ-RKT on AP-1 transcription factor activation in AGEs-treated H9c2 cells.
(a) Phospho-c-Jun DNA binding activity. (b) c-Fos DNA binding activity. (c) FosB DNA binding activity. (d) JunD DNA binding activity.
(C) Immunoblot expression of phospho-c-Jun in AGEs-treated H9c2 cells.
(a, and b) Effect of IQ-RKT on phospho-c-Jun in MGO-, and Glu-AGEs treated cells. (c, and d) Quantification of phospho-c-Jun signals.
(D) (a) Immunoblot analysis of phospho-c-Jun expression in heart tissues of diabetic rats. (b) Quantification of phospho-c-Jun levels.
(E) (a) IQ-RKT inhibited p65/RelA activation in AGEs-treated H9c2 cells. (b) IQ-RKT inhibited c-Rel activation in AGEs-treated H9c2 cells.
(F) (a) Immunoblot of p65 (Ac-RelA (lys310)) in heart tissues of diabetic rats. (b) Quantification of p65 (Ac-RelA (lys310)) signals.

Figure 9: IQ-RKT Enhances anti-apoptotic Bcl-2 expression, and inhibits pro-apoptotic Bax expression in cardiomyocytes.
(A) (a) Immunocytochemistry of Bax (merged) in AGEs-stimulated H9c2 cells, and pre-treated IQ-RKT cells. Also see separate channels Texas Red, and DAPI (Figure S5). (b) MFI of Bax in AGEs-treated H9c2 cells, and pre-treated IQ-RKT cells.
(B) (a) Immunostained sections of diabetic heart, and treatment groups. Circles represent the Bax protein expression in cardiac tissue. (b) MFI of Bax signals in heart tissues of diabetic rats, and treatment groups.
(C) (a) Immunocytochemistry of Bcl-2 (merged) in AGEs-treated H9c2 cells, and pre-treated IQ-RKT cells. Also see separate channels FITC, and DAPI (Figure S6). (b) MFI of Bcl-2 in H9c2 cardiomyocytes.
(D) (a) Immunostained segments of diabetic heart, and treatment groups. Circles indicate the expression of Bcl-2 protein in heart tissue. (b) MFI of Bcl-2 expression in heart tissues of diabetic rats, and treatment groups.

Figure 10: IQ-RKT Exhibits anti-apoptotic effects by diminishing caspase-3 activation.
(A) Time course curve of caspase-3/-7 activity in AGEs-stimulated H9c2 cells.
(B) Assessment of caspase-3/-7 activity in AGEs-treated H9c2 cells, pre-treated with IQ-RKT.
(C) Qualitative analysis of caspase-3/-7 activation in H9c2 cardiomyocytes *via* immunocytochemical study.
(D) (a) Immunoblot expression of active caspase-3 in diabetic heart tissues. (b) Active caspase-3 signal levels in diabetic heart tissues.

Figure 11: IQ-RKT effect on glucose metabolism in non-diabetic rats.
(A) Glucose metabolism activity in normal rats.
(B) Effect of AG on glucose metabolism.
(C) Effect of metformin on glucose metabolism.
(D) Effect of IQ-RKT on glucose metabolism.

Figure 12: Impact of pH and temperature on the stability of IQ-RKT along with microelectronic changes monitored by NMR spectroscopy.

(A) Changes in pH (2, 6.8, 7, and 10) showed no effect on the stability of IQ-RKT.
(B) Stability of IQ-RKT did not alter at different temperatures, and was found stable up to 50° C.
(C) ^{1}H-NMR spectra of three components, and formulation IQ-RKT at 50° C recorded at 400 MHz, showed no change in chemical shifts of any component in mixture, thus indicating no intermolecular interactions among kaempferol, rutin, and thymoquinone.

- Formulation IQ-RKT (a 1/3 composition of Rutin, Kaempferol, and Thymoquinone)

Figure 13: Summary of IQ-RKT protective effects on the AGE-RAGE-induced apoptotic pathway in cardiomyocytes *in vitro*, and *in vivo*.

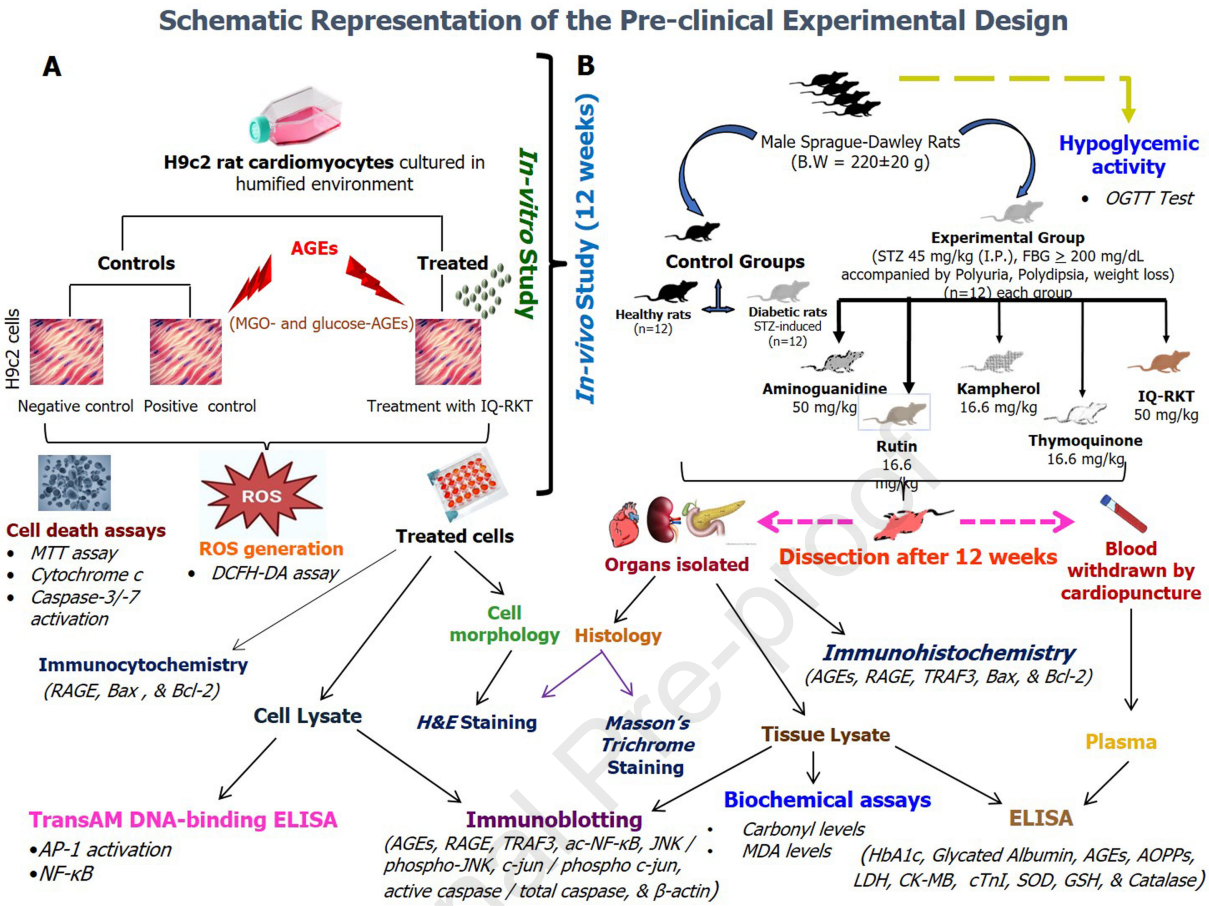

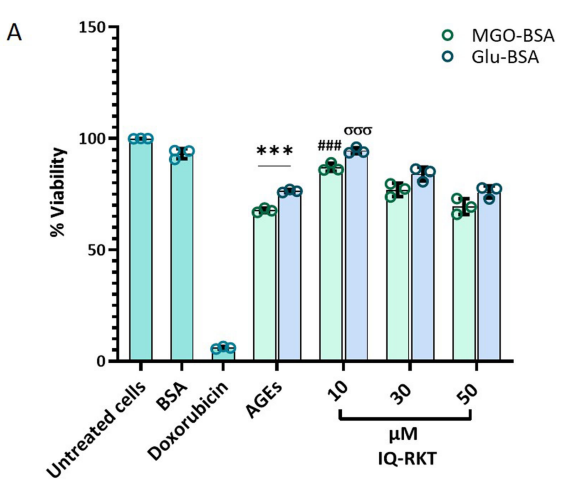

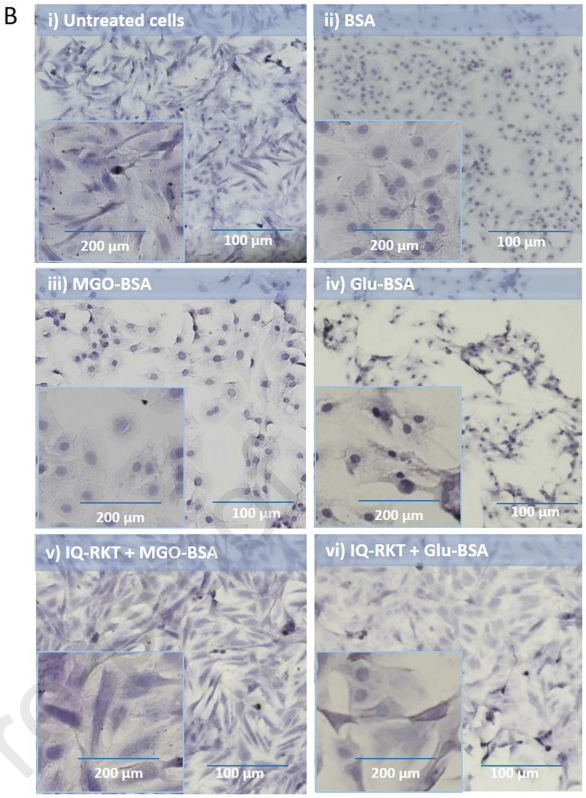

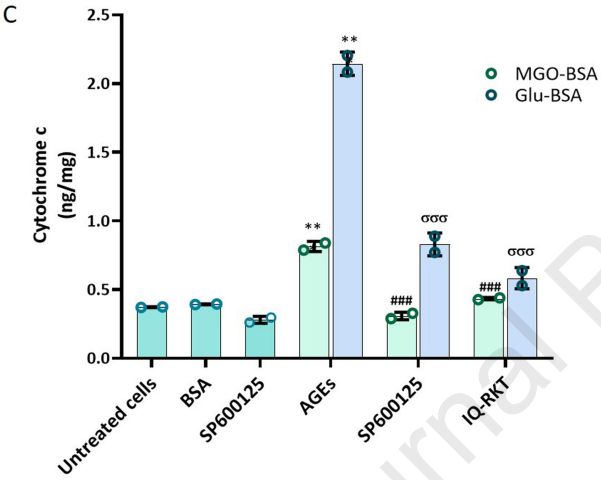

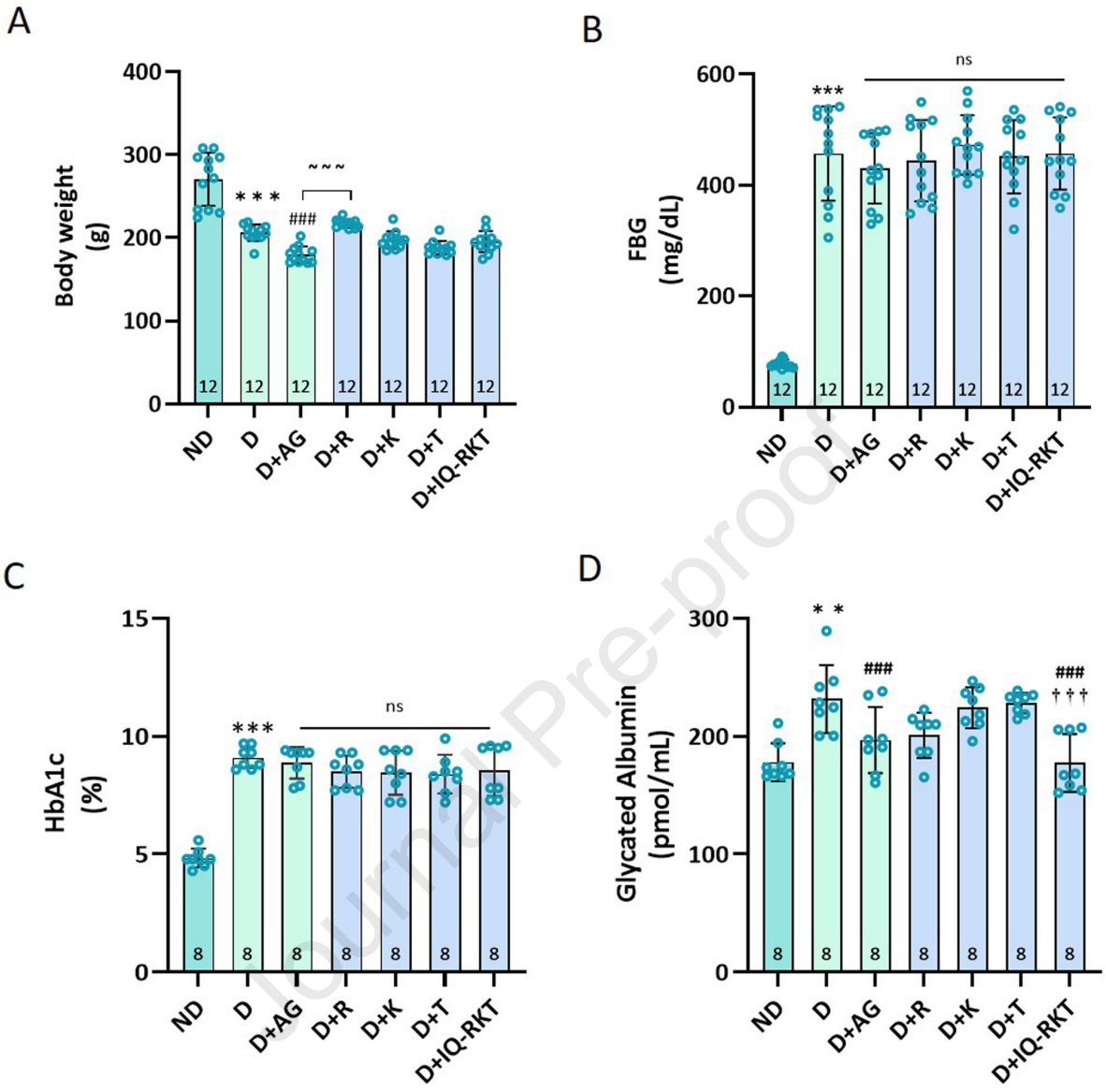

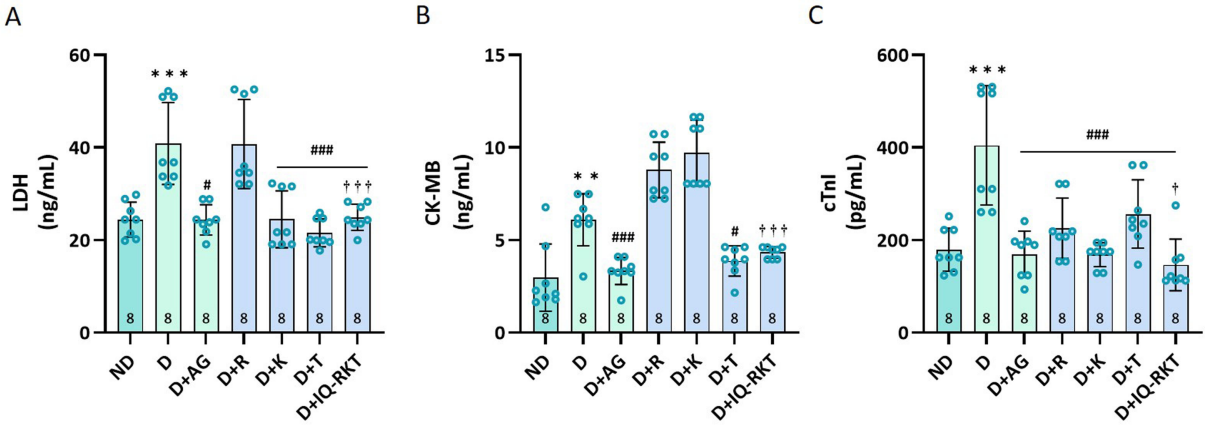

6A

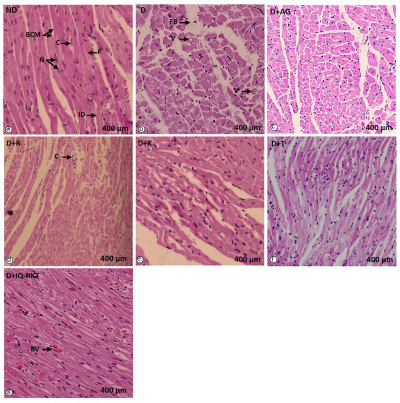

6B

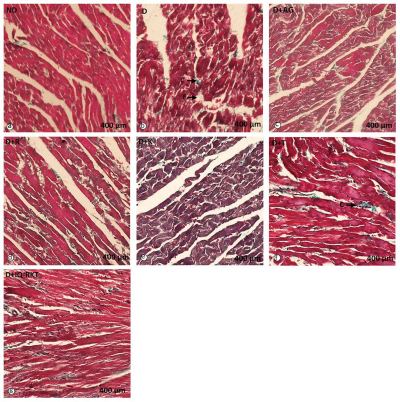

6C

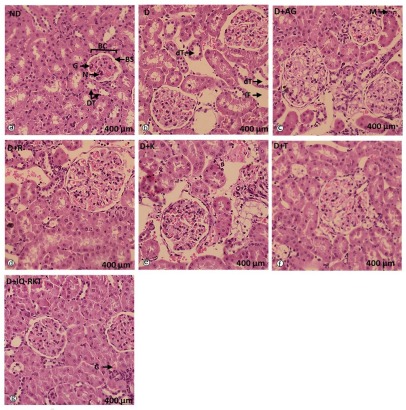

6D

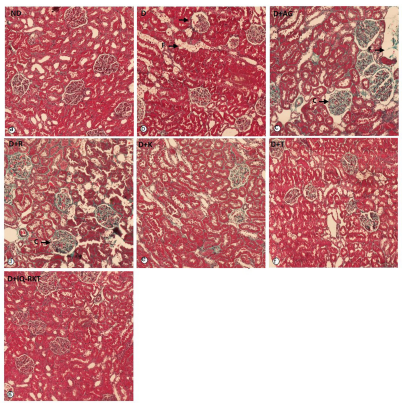

6E

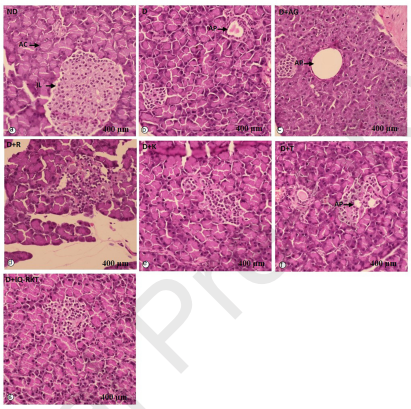

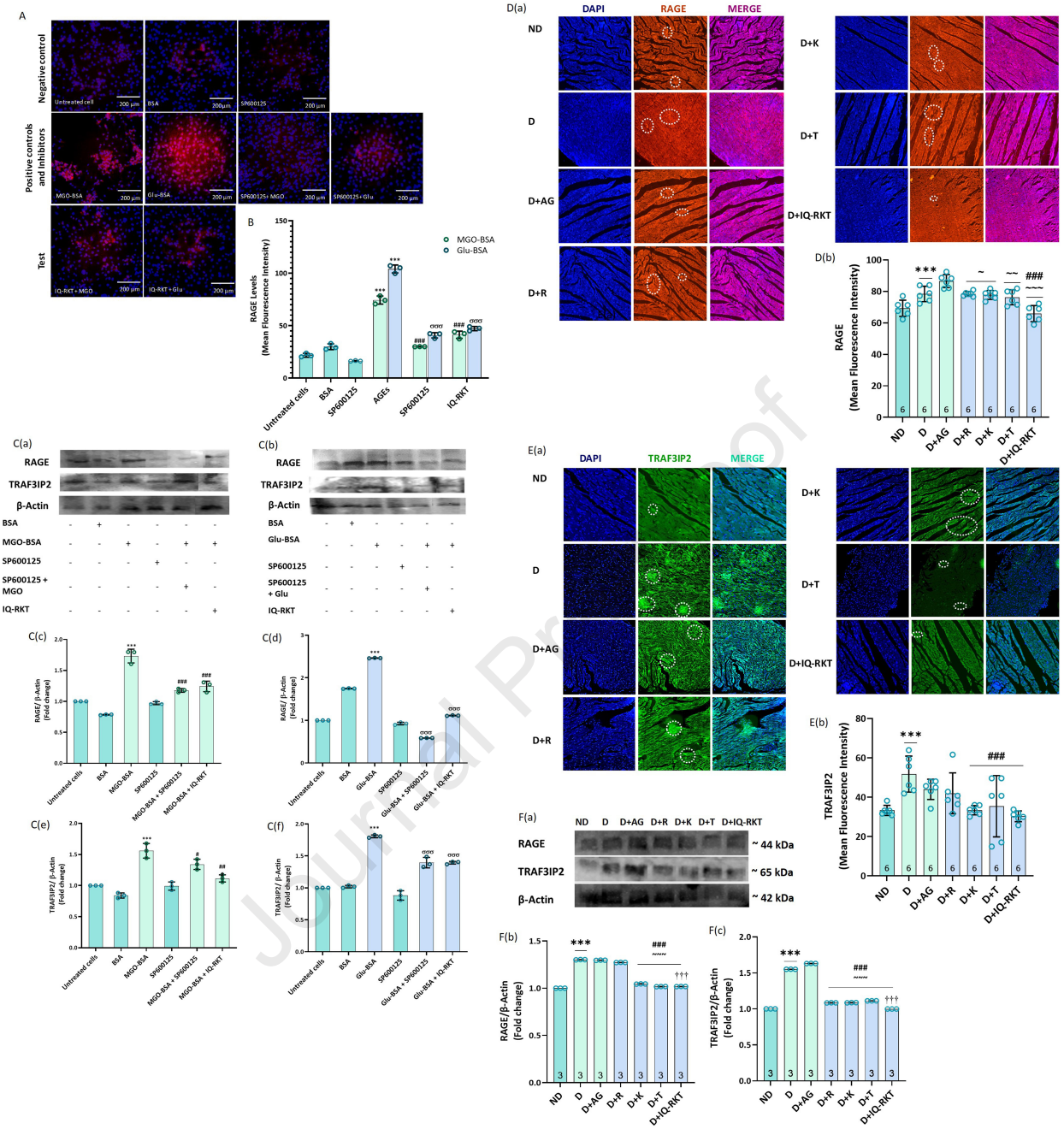
A
Negative control
Positive controls and Inhibitors
Test
Untreated cell
BSA
SP600125
MGO-BSA
Glu-BSA
SP600125+ MGO
SP600125+ Glu
IQ-RKT + MGO
IQ-RKT + Glu
200 µm
B
MGO-BSA
Glu-BSA
RAGE Levels (Mean Flourescence Intensity)
Untreated cells
BSA
SP600125
AGEs
SP600125
IQ-RKT
C(a)
RAGE
TRAF3IP2
β-Actin
BSA
MGO-BSA
SP600125
SP600125 + MGO
IQ-RKT
C(b)
RAGE
TRAF3IP2
β-Actin
BSA
Glu-BSA
SP600125
SP600125 + Glu
IQ-RKT
C(c)
RAGE/ β-Actin (Fold change)
Untreated cells
BSA
MGO-BSA
SP600125
MGO-BSA + SP600125
MGO-BSA + IQ-RKT
C(d)
RAGE/ β-Actin (Fold change)
Untreated cells
BSA
Glu-BSA
SP600125
Glu-BSA + SP600125
Glu-BSA + IQ-RKT
C(e)
TRAF3IP2/ β-Actin (Fold change)
Untreated cells
BSA
MGO-BSA
SP600125
MGO-BSA + SP600125
MGO-BSA + IQ-RKT
C(f)
TRAF3IP2/ β-Actin (Fold change)
Untreated cells
BSA
Glu-BSA
SP600125
Glu-BSA + SP600125
Glu-BSA + IQ-RKT
D(a)
DAPI
RAGE
MERGE
ND
D
D+AG
D+R
D+K
D+T
D+IQ-RKT
D(b)
RAGE (Mean Fluorescence Intensity)
ND
D
D+AG
D+R
D+K
D+T
D+IQ-RKT
E(a)
DAPI
TRAF3IP2
MERGE
ND
D
D+AG
D+R
D+K
D+T
D+IQ-RKT
E(b)
TRAF3IP2 (Mean Fluorescence Intensity)
ND
D
D+AG
D+R
D+K
D+T
D+IQ-RKT
F(a)
ND
D
D+AG
D+R
D+K
D+T
D+IQ-RKT
RAGE
TRAF3IP2
β-Actin
~ 44 kDa
~ 65 kDa
~ 42 kDa
F(b)
RAGE/β-Actin (Fold change)
ND
D
D+AG
D+R
D+K
D+T
D+IQ-RKT
F(c)
TRAF3IP2/β-Actin (Fold change)
ND
D
D+AG
D+R
D+K
D+T
D+IQ-RKT

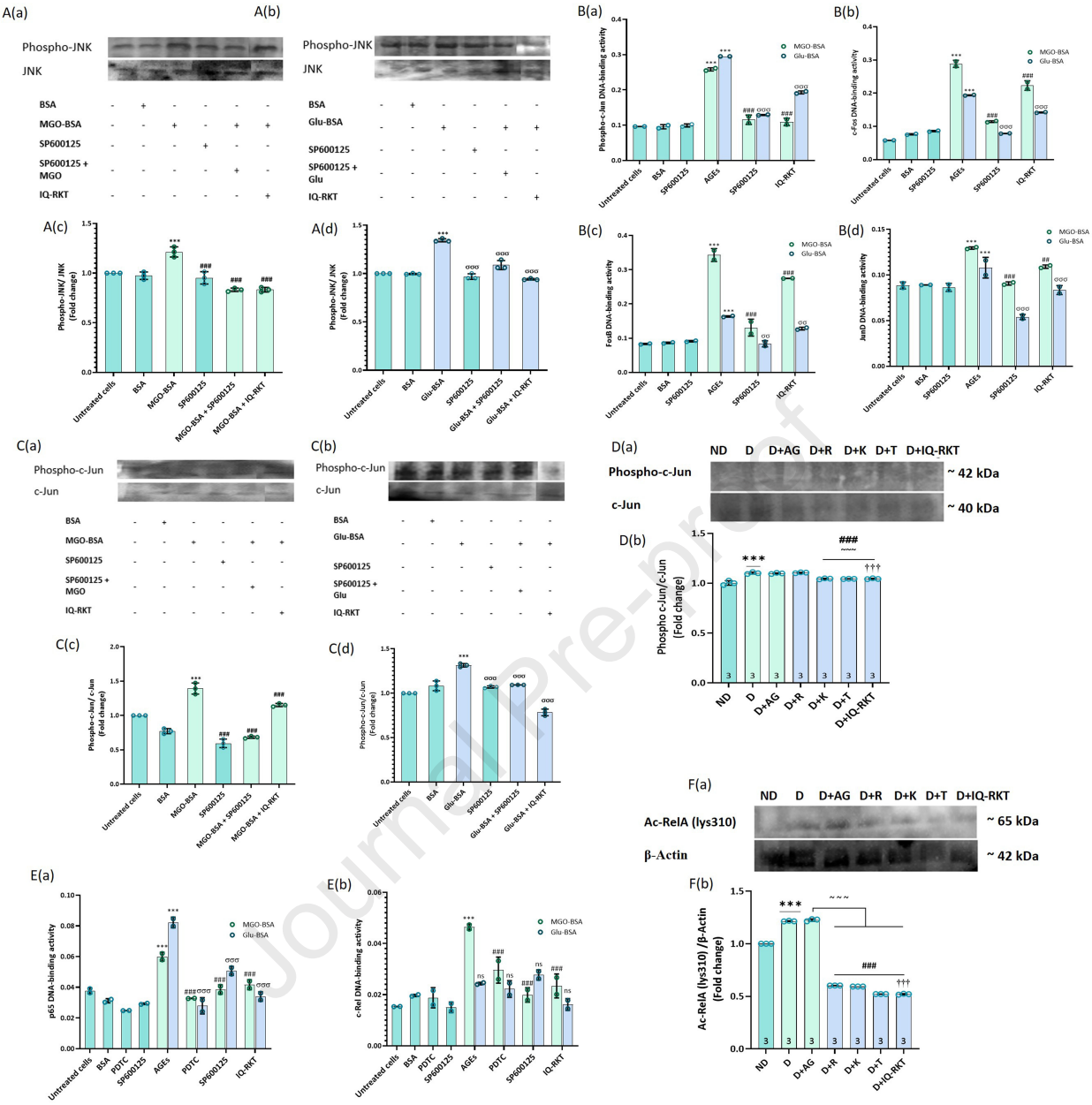

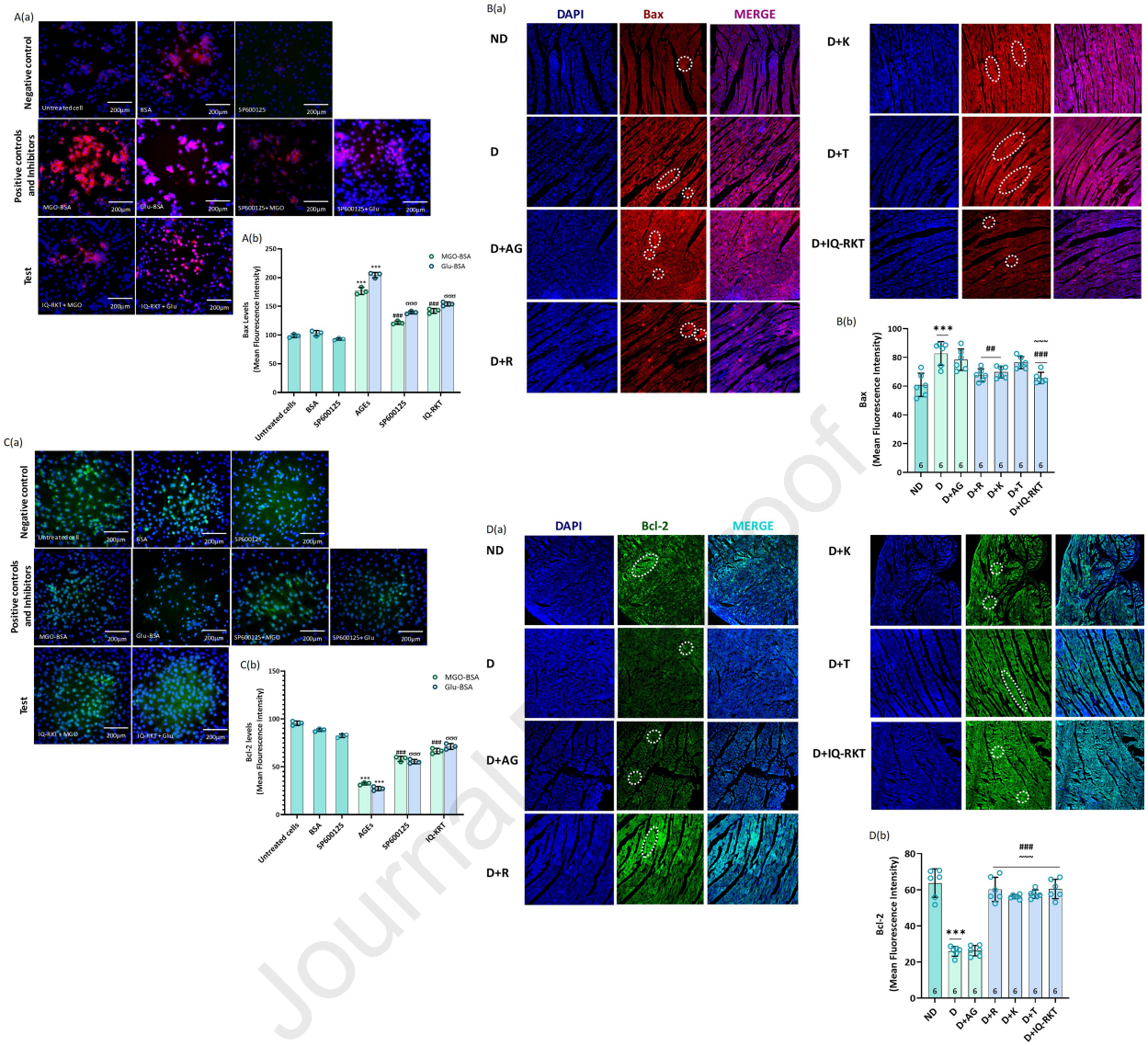

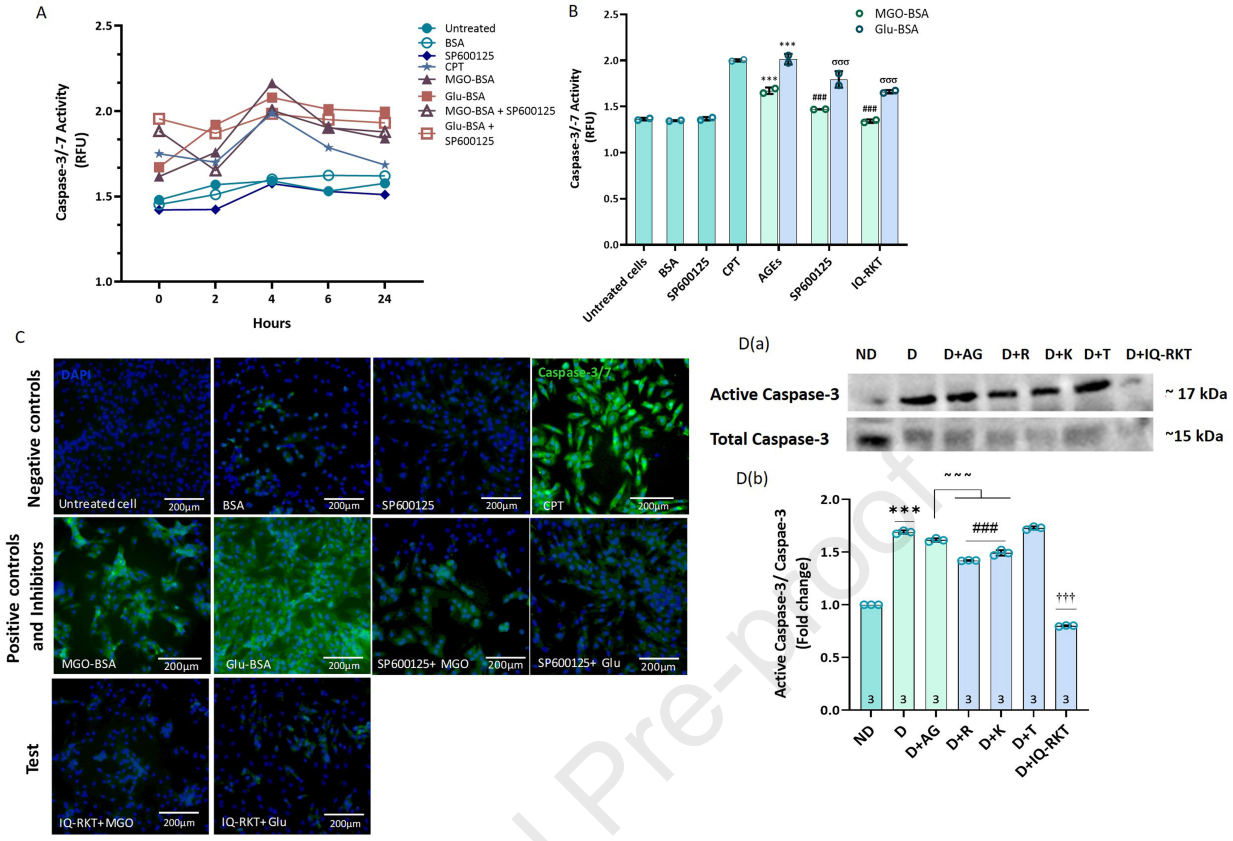

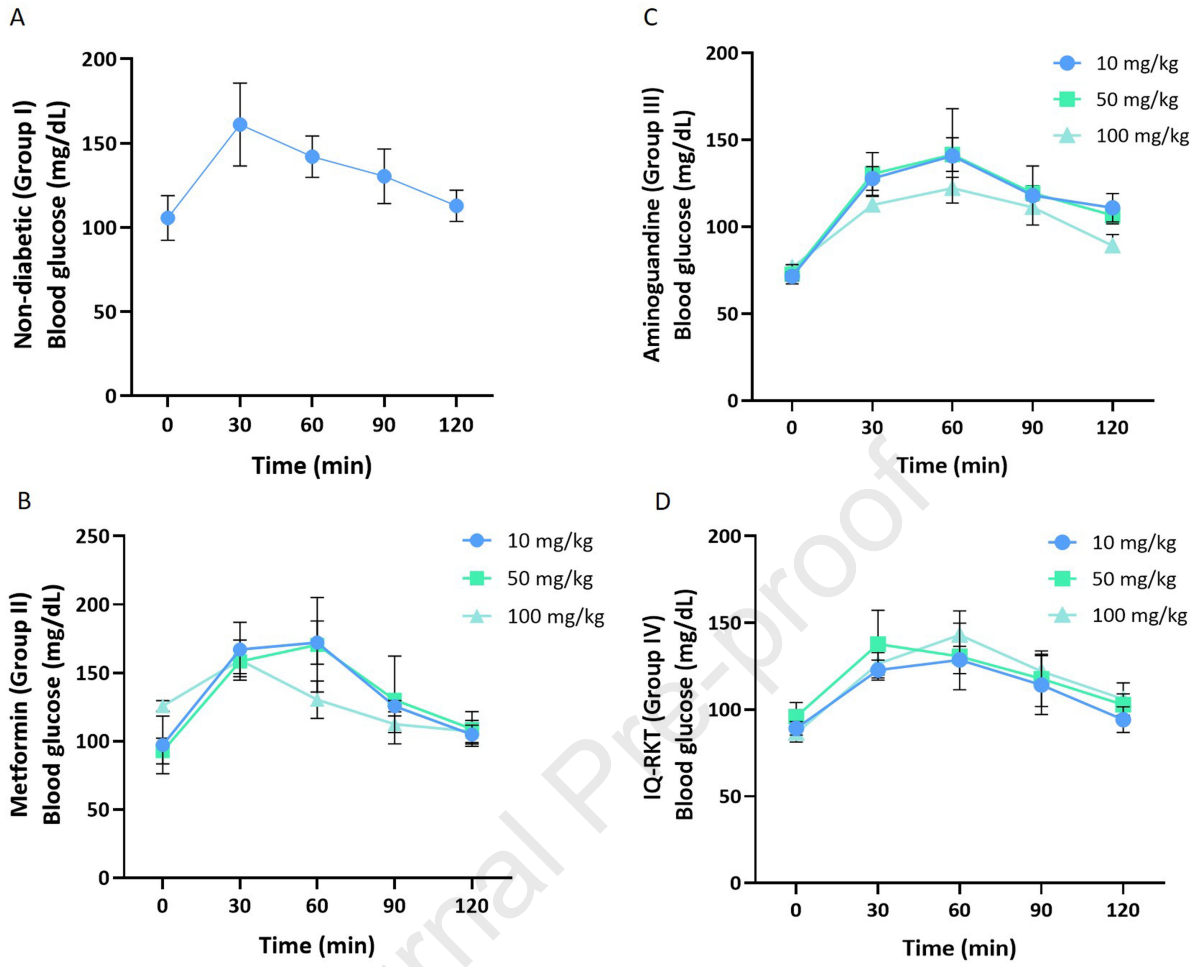

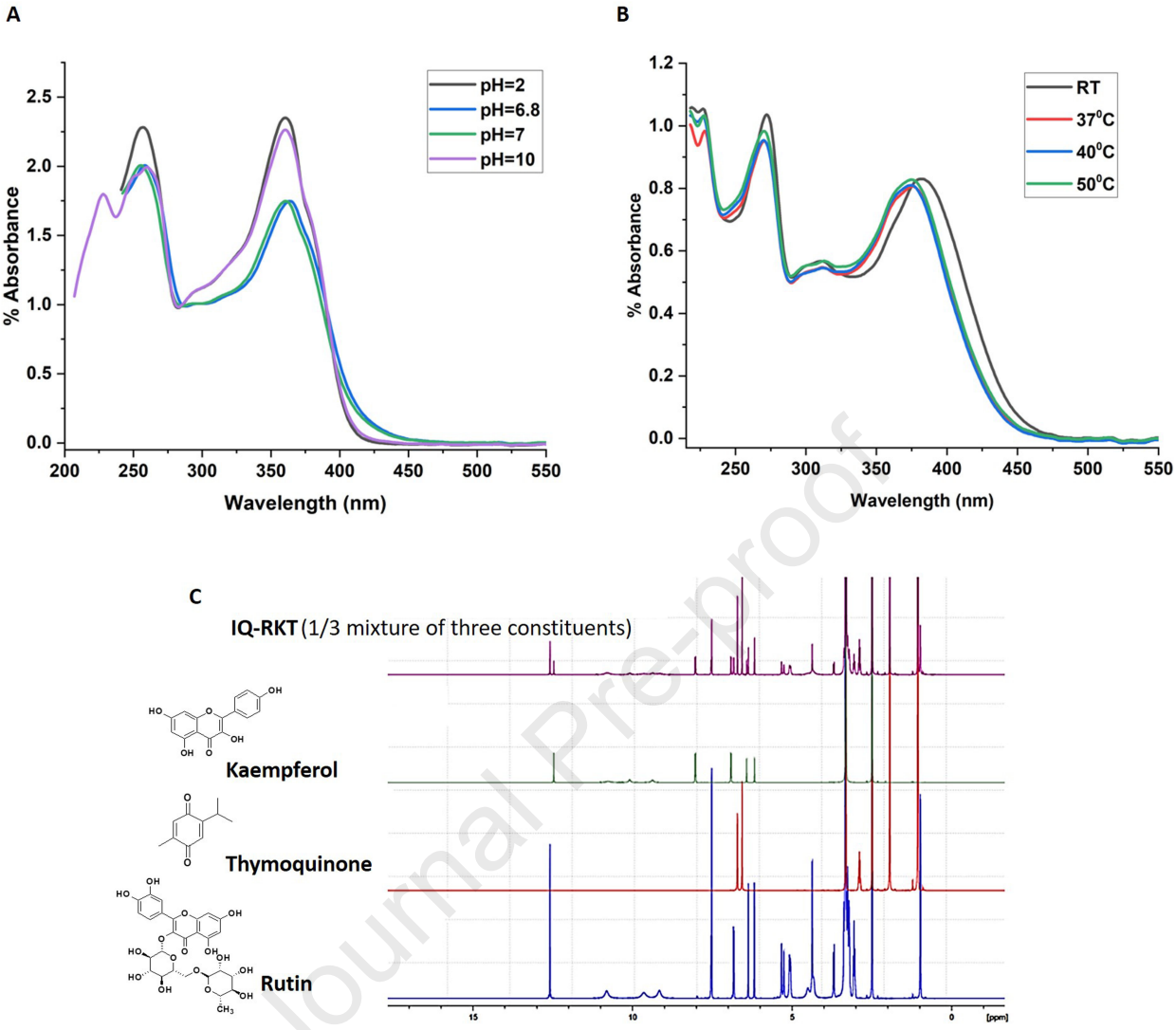

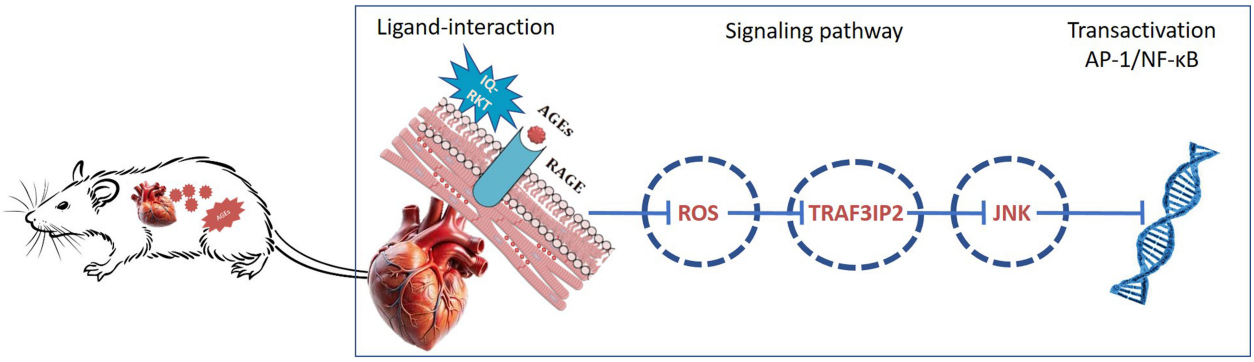

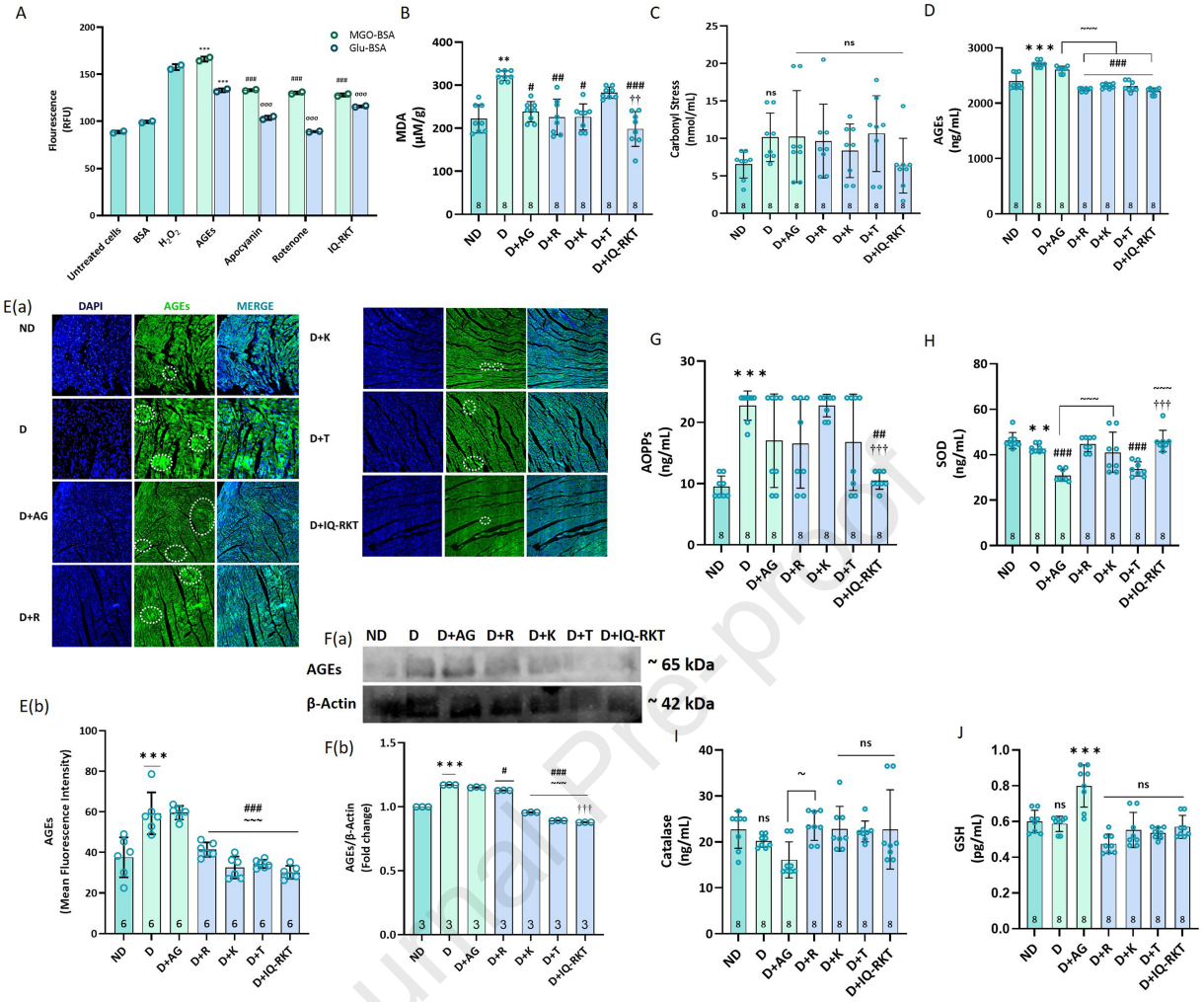

Conflict of Interest

The authors have declared no conflict of interest

Corresponding authors: Dr. Humera Jahan, and Prof. Dr. M. Iqbal Choudhary